# ELUCIDATING THE DYNAMICS AND ROLE OF MACROPHAGES IN A MURINE MODEL OF ELASTASE-INDUCED EMPHYSEMA

Amy Kathryn Poupore

Department of Molecular Microbiology and Immunology

Johns Hopkins Bloomberg School of Public Health

A thesis submitted to Johns Hopkins University in conformity with the requirements for the degree of Master of Science

Baltimore, Maryland

May 2016

# ABSTRACT

Emphysema is a complex immunological disease characterized by progressive and irreversible damage to the parenchymal lung tissue. While the cause of the disease can most often be attributed to habitual cigarette smoking or long-term exposure to other toxic substances, the underlying mechanisms of the pathogenesis are poorly understood. Of particular interest is why alveolar destruction continues to occur even after cessation of smoking. Data from human patient samples and laboratory animals have implicated a role for macrophages as they are a long-lived, abundant cell within the alveolar space that has the ability to secrete many of the damaging enzymes associated with tissue destruction. The importance of macrophages and their dynamics in the progression of emphysema are not, however, well understood. This work seeks to delineate the early myeloid cell dynamics in a murine elastase-induced emphysema model and to address the hypothesis that the early alterations in lung macrophage phenotype contribute to the progression of tissue destruction in this model.

To elucidate the dynamics of macrophages, monocytes, and neutrophils in the lung, BALB/cJ mice were administered 3 enzymatic units of porcine pancreatic elastase and their lungs were analyzed via flow cytometry at various time points throughout the two-weeks following elastase administration. To evaluate the importance of lung macrophages during the acute period following elastase administration, macrophages were depletion by giving a total of three doses of clodronate-loaded liposomes. The effect of depletion on emphysema severity was determined by performing pulmonary function tests 21 days post-elastase.

As expected, neutrophils and monocytes infiltrated the lung during the acute inflammatory phase, peaked around day 2 and 4, respectively, and returned to baseline by day 14 post-elastase. Resident alveolar macrophages underwent an initial contraction, followed by a slight proliferation, and by day 14 there were marginally fewer cells than in the naïve lung. Interstitial macrophages on the other hand proliferated and peaked by day 4 post-elastase and gradually declined to be somewhat elevated above baseline.

Pulmonary function tests revealed that the depletion of macrophages worsened emphysema severity. This work supports the hypothesis that macrophages play a significant role in emphysema progression, however it does not address the mechanism of action. Future research using macrophage reprogramming may help address this.

# ACKNOWLEDGEMENTS

When I applied to do my master's at the Johns Hopkins School of Public Health, I was certain that I wanted to work in malaria or at the very least, some infectious disease. That is of course until I took my first immunology class with Dr. Alan Scott where I grew to love immunology and ended up doing chronic lung disease research in his lab. It's no wonder that Dr. Scott wins the Golden Apple teaching award every year he's eligible; his dedication and passion for immunology, pedagogy, and mentorship are inspiring and have guided my decision to pursue a career as an immunologist. I am sincerely grateful to Dr. Scott for the opportunity to complete my master's research in his laboratory and for his guidance, patience, and enthusiasm that have inspired me and allowed me to grow as a scientist.

Upon joining the Scott lab, I had no experience working with animals and very little experience even using a pipette, much less doing flow cytometry. The work herein would not be possible without the training I received from my many mentors at Hopkins. To Drs. J. Matt Craig, Dan Lagassé, Nathachit "James" Limjunyawong, Stephane Lajoie and all of the other scientists at Hopkins that I've had the honor of learning from, I am forever grateful. Aside from teaching me everything I know at the bench and much of what I understand in immunology, I am particularly thankful to Matt for making the lab a source of enjoyment. Even though it was only the two of us, I'm pretty sure we had more fun running flow while bumping Flo Rida than any other lab in the department. I would also like to give special thanks to James, Dr. Wayne Mitzner, and the rest of the Mitzner lab for all of their help and guidance in obtaining and analyzing pulmonary function data and for educating me in respiratory physiology.

Lastly, I must thank my parents for their support and encouragement as well as all of the incredible, fun, intelligent people I've met during my tenure at Johns Hopkins who have made graduate school a blast.

This work was supported by the National Heart, Lung, and Blood Institute (NHLBI) of the National Institutes of Health (NIH) through grants P01HL10342

# PREFACE

Chronic obstructive pulmonary disease is a heterogeneous lung disease that comprises obstructive bronchitis, affecting the conducting airways, and emphysema, affecting the lower respiratory airways[1]. Emphysema, the focus of this thesis, is defined by a progressive and irreparable destruction of alveolar tissue, resulting in impaired lung function. The most common symptoms associated with COPD are dyspnea, chronic cough, excess sputum production, and fatigue.

Chronic obstructive pulmonary disease poses a significant public health burden; over 65 million people are living with the disease worldwide and in 2012 the World Health Organization named COPD the third leading cause of death worldwide[2]. Due to the chronicity of the disease and its impact on the ability to perform tasks of daily living, COPD has one of the highest global years lost to disability[3].

Considering its significant strain on society, our progress toward understanding the cellular and molecular basis of this complex immunological disease is lagging. Further, the limited number of available treatments only ameliorate symptoms but do nothing to abate the underlying disease[4]. In order to develop treatments that allay the continued tissue destruction, knowledge into the mechanisms of emphysema progression is necessary.

The overall aim of this thesis is to contribute to the understanding of the immune environment in the emphysematous lung and its role in the progressive destruction of parenchymal tissue. Specifically, this work focuses on identifying the dynamics and role of macrophages in a murine model of progressive emphysema. The thesis will begin with background information to orient the reader to lung structure and function, COPD/emphysema, animal models of emphysema, the current understanding of

emphysema pathogenesis, and lastly the specific aims of this work. Part 1 of the results section will describe the dynamics of resident and recruited macrophages, monocytes, and neutrophils in the murine lung following elastase administration and Part 2 will detail the effect of resident macrophage depletion on the progression of elastase-induced emphysema. The thesis will conclude with a discussion on the implications of this research and future directions.

# TABLE OF CONTENTS

# TABLES

# FIGURES

# INTRODUCTION

## Structure and function of the respiratory system

*Gross anatomy*

Oxygen is required for energy production by most tissues in the mammalian body, thus continuously providing cells with oxygen from the environment and removing carbon dioxide produced during aerobic metabolism is integral to the body's proper functioning. This homeostasis is maintained by the respiratory system, comprised of the conducting airways, lungs, and chest wall.

The airways and their associated blood vessels are composed of branching structures that narrow and shorten as they eventually infiltrate the entire lung parenchyma[5,6]. Inspired air first passes through the upper airways including the nose or mouth, pharynx, and larynx, and then enters the lower airways of the lung via the tracheobronchial tree. The dichotomously branching airways in humans begin with the trachea (generation 0) which bifurcates into the left and right mainstem bronchi (1$^{st}$ generation) at an approximately $45^0$ angle at the carina, entering into the left and right lungs, respectively. In humans, there are three right lung lobes and two left lung lobes and in mice there are four right lung lobes and one left lung lobe. The bronchi continue to branch into bronchioles, respiratory bronchioles, alveolar ducts, and end as alveolar sacs, over the course of 23 generations in humans. Unlike humans, mice have monopodial branching, lack cartilage in the conducting airways beyond the mainstem bronchi, and lack respiratory bronchioles, resulting in only 13-17 generations[5] (**Figure 1**).

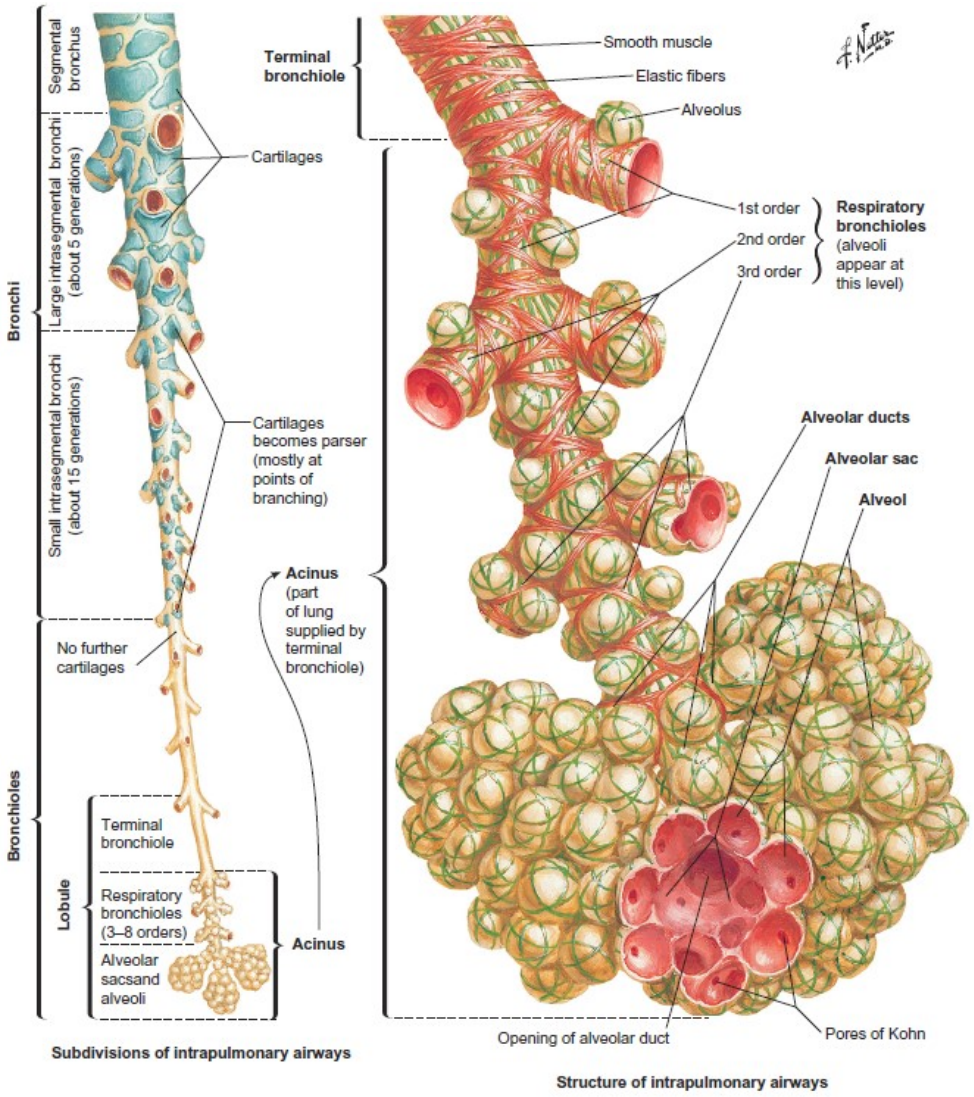


**FIGURE 1 Conducting airways and respiratory zone of human lung** Reproduced from Elseveier Inc. www.netterimages.com[5], Copyright (2011).

In humans, the nose/mouth through the first 15 generations of branching airways comprise the conducting zone where the air is filtered, moistened, and heated as it is directed to the remaining 8 generations that comprise the acinus. Because the conducting airways are unable to facilitate gas exchange, they are referred to as the anatomical dead space, where the final portion of each inspiration remains without any change in composition[6,7]. The acinus begins with the respiratory bronchioles, containing a few evaginations or alveoli capable of gas exchange, and

leads to the alveolar ducts, culminating in the main respiratory zone composed of many alveolar sacs[7,8].

The branching pattern of the airways is mirrored by that of the pulmonary arteries with each bronchus or bronchiole closely associated with its respective artery or arteriole. In humans, the pulmonary veins travel to the left atrium peripherally to the bronchi whereas in mice, they follow a similar course to the bronchi. At the level of the alveoli, a dense mesh-like network of capillaries envelopes each alveolar sac, creating an environment conducive to efficient gas exchange. Blood in the capillary network is separated from inspired air by a thin tissue membrane of capillary endothelium and alveolar epithelium, just 0.6 μM thick in humans or 1/13$^{th}$ the diameter of an erythrocyte. Additionally, capillary beds are sandwiched between alveolar saccules and thus surrounded by air on both sides, further facilitating the exchange of oxygen in the air for carbon dioxide in the blood[9].

In order to ensure that this exchange is efficient as possible, the alveoli must be structured to achieve an extremely large surface area with an appropriately thin barrier between the alveolar air and capillary blood. Adult human lungs contain around 480 million alveoli[10] resulting in an internal surface area of 24-81 $m^2$, varying by height of the individual[11–13]

*Cellular environment*

Whereas the capillary endothelium consists of a uniform layer of squamous cells, the alveolar membrane wall is a mosaic of two distinct types of alveolar epithelial cells or pneumocytes. Each of the 400 million or so alveoli in the human lung are comprised of about 40 type I cells and 77 type II cells. Though type I cells account for only 34% of epithelial cells in the membrane, they are an impressive form of squamous cell that manage to cover over 95% of the surface. Each type I cell covers a surface area of 5,100 $\mu m^2$ via multiple large cytoplasmic extensions that surround and transverse alveolar septa[14](**Figure 2**).

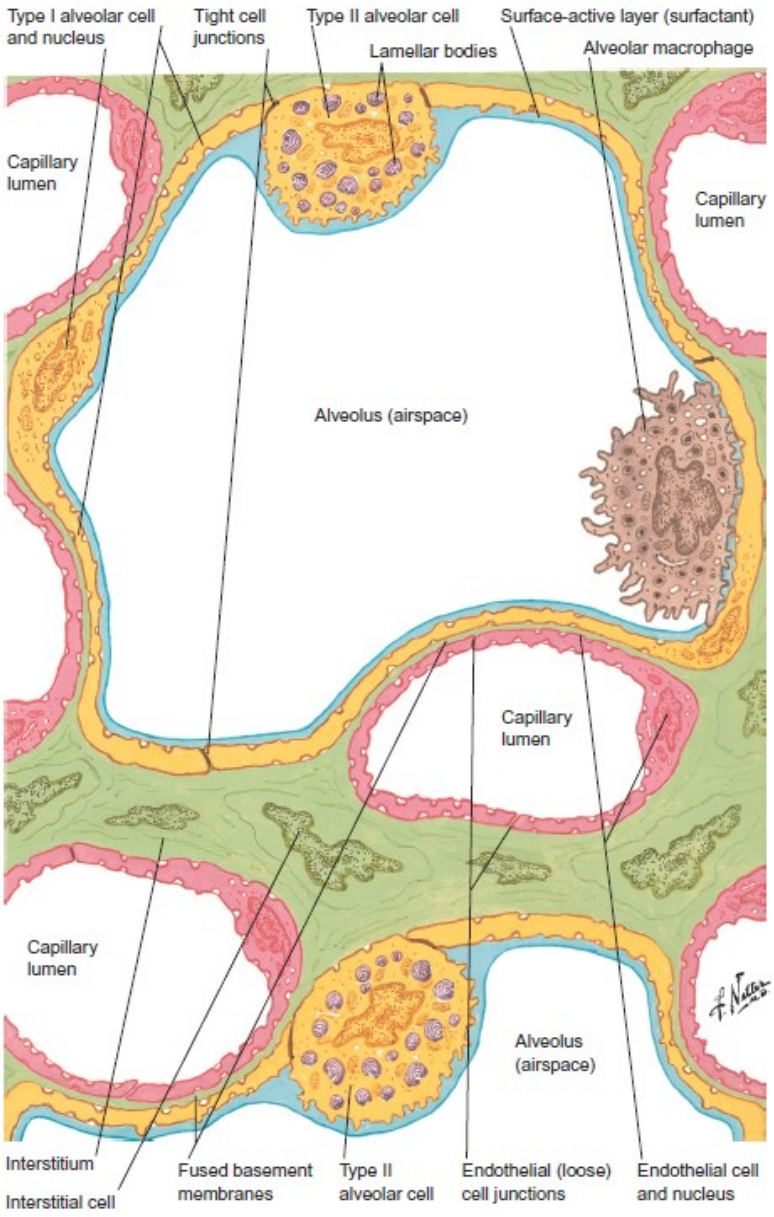


**FIGURE 2 Mammalian alveolus** Reproduced from Elsevier Inc. www.netterimages.com[5], Copyright (2011).

Interspersed among type I cells are the cuboidal type II cells, representing approximately 66% of alveolar epithelial cells and covering just 5% of the alveolar surface area[15]. They are distinct from type I cells given their many phospholipid-rich lamellar bodies and apical microvilli that secrete interstitial fluid. While type I cells give rise to the alveolar membrane's facilitation of gas exchange, type II cells maintain and protect the alveolar environment. They prevent atelectasis

through the release of surfactants, replace damaged epithelium through self-renewal and transdifferentiation, avoid alveolar edema through transepithelial sodium transport, and limit inflammation and microorganisms through the release of anti-inflammatory and anti-microbial substances such as surfactant protein-A and lysozyme[15,16].

To maintain the basement membrane of the epithelium, underlying fibroblasts produce extracellular matrix components including collagen and elastin fibers, fibronectin fibrils, and proteoglycans[17,18]. Additionally, the alveolar space contains specialized immune cells including alveolar macrophages and a small number of lymphocytes[19] (**Figure 3**). These cells partake in both the innate and adaptive immune systems and alter their phenotype from baseline in the context of infection and injury.

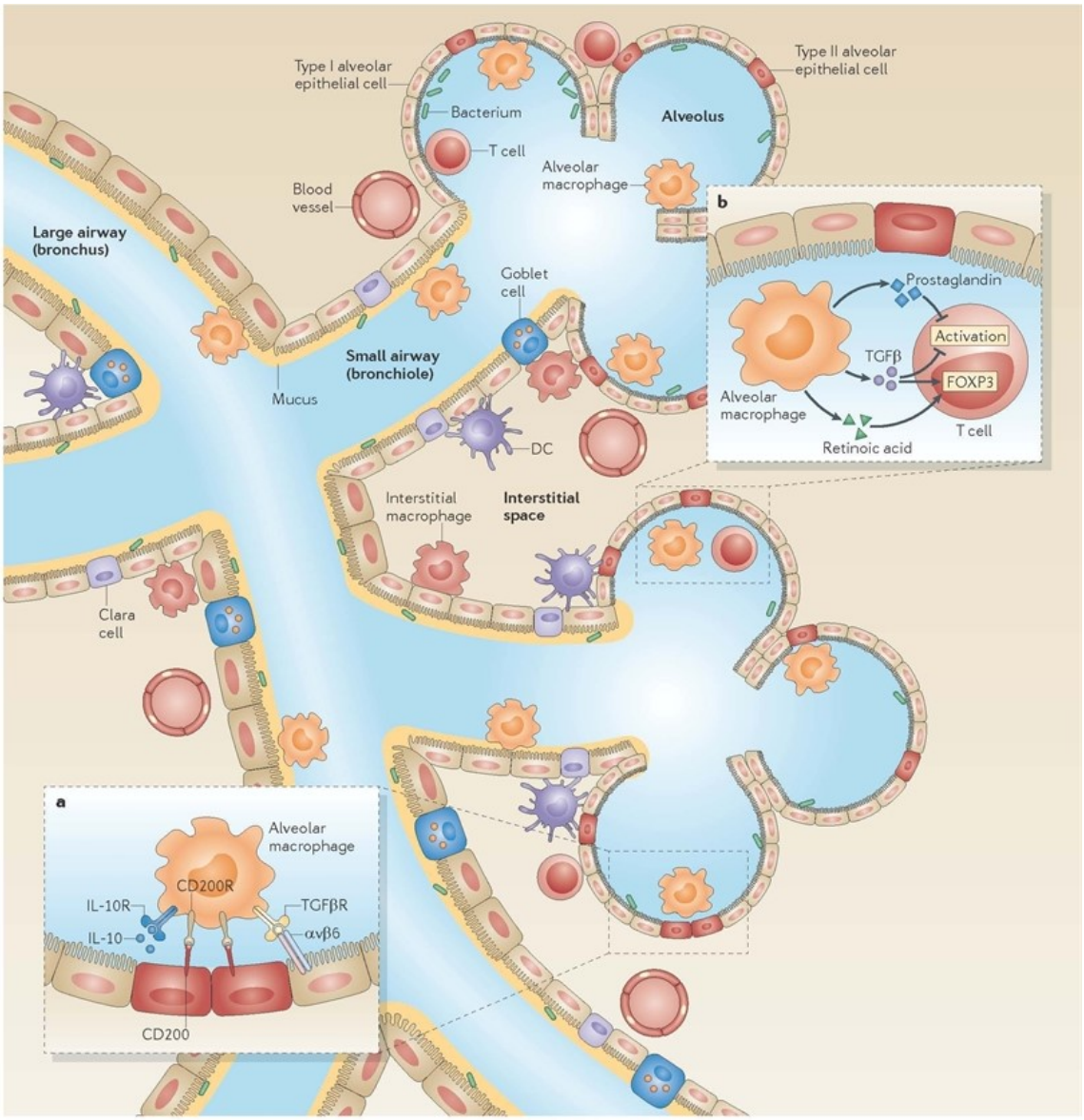


**FIGURE 3 Leukocytes in the respiratory zone of the lung** Reproduced from Macmillan Publishers Ltd: Nature Reviews Immunology[19], Copyright (2014).

*Lung macrophages*

The lung contains at least three distinct macrophage subsets: bronchial macrophages in the conducting airway, alveolar macrophages in the respiratory airway, and interstitial macrophages in the interstitial space between the alveolar epithelium and capillary endothelium. Pulmonary macrophages act to eliminate debris, apoptotic cells, and microorganisms from the

lung and play significant roles in the promotion and suppression of inflammation as well as wound healing and airway remodeling[19,20].

Up until recently, the paradigm for the origin of tissue resident macrophages was that they were part of a unified mononuclear phagocyte system (MPS) that was maintained at steady-state by circulating monocytes that differentiate into tissue-specific macrophages. However, cellular fate mapping experiments have demonstrated that these tissue resident macrophages are partially to not-at-all of hematopoietic or monocytic origin[21,22]. Further, the observation that tissue macrophages appear during embryogenesis prior to the appearance of monocytes creates a temporal challenge to the MPS paradigm[22,23]. From 2010 until the present, several groups determined that resident tissue macrophages including microglia in the brain, Langerhans cells in the skin, Kupffer cells in the liver, and peritoneal, kidney, and splenic macrophages were not of adult hematopoietic origin and were likely derived from the fetal yolk sack. In 2013, Guilliams et al. delineated the alveolar macrophage origin to be of $Ly6C^{hi}$, $CD11b^{hi}$ fetal monocytes that colonize the developing lung at day E16.5 and subsequently begin differentiating into alveolar macrophages around E18.5, during the saccular stage of lung development[24]. Maturation of these cells occurs within 3 days of birth and the entire process is largely dependent on granulocyte macrophage-colony stimulating factor (GM-CSF). This population, comprising 90-95% of leukocytes in the alveolar space, is maintained through self-renewal in steady state conditions and has a half-life of approximately 12-months[24–26].

Conversely, interstitial macrophages have a high turnover rate at steady-state and are posited to be replenished by circulating $Ly6C^{-}$ monocytes[27]. Some groups suggest that in circumstances where alveolar macrophages are depleted (either through infection[28], experimental depletion, or irradiation prior to bone marrow transplant[29]), interstitial macrophages differentiate into alveolar macrophages and are replenished by blood monocytes. Landsman and Jung reported that following depletion of alveolar macrophages, $Ly6C^{-}$ monocytes are recruited to the interstitial

space, differentiate into an intermediate interstitial macrophage, undergo proliferative expansion, and then migrate into the alveolar space[30].

As the lung is a delicate organ that relies on the patency of the airways for efficient gas exchange, alveolar macrophages ideally maintain the sterility of the lung while limiting inflammation. Because they exert such a significant presence in the lung, alveolar macrophages are the main orchestrator of the pulmonary immune environment and interact intimately with alveolar epithelial cells and T cells[19,26]. They highly express many anti-inflammatory proteins including CD200R that binds CD200 (OX-2) expressed on type II alveolar epithelial cells, endothelial cells, B cells, and some T cells to inhibit macrophage responsiveness to toll-like receptors (TLRs) and signal-regulatory protein-α (SIRP-α) that binds surfactant proteins A and D to inhibit macrophage phagocytosis at baseline and can also bind CD47 to prevent inflammation during macrophage phagocytosis of erythrocytes[31]. Further, alveolar macrophages express various scavenger receptors that sequester damage-associated molecular pattern molecules (DAMPs), pathogen-associated molecular pattern molecules (PAMPs), and complement to aid in the clearance of pathogens. Alveolar macrophages also play a role in the adaptive immune response by promoting tolerance to harmless antigens via poor antigen presentation to T cells and a lack of costimulatory molecules. Additionally, they secrete transforming growth factor (TGF)-β, anti-inflammatory prostaglandins, and retinoic acid that can suppress dendritic cells from activating effector T cells or skew them toward the development of forkhead box P3 $(FOXP3)^+$ regulatory T cells[19]. While alveolar macrophages suppress inflammation at steady-state, in response to the repeated injury that is incurred with habitual cigarette smoking or indoor burning of biomass fuels, alveolar macrophages seem to orchestrate a pro-inflammatory, destructive lung environment that results in COPD and emphysema.

**Chronic Obstructive Pulmonary Disease**

*Defining features*

Chronic obstructive pulmonary disease (COPD) is characterized by irreversible progressive airflow limitation and is comprised of a mix of small airway disease, including chronic obstructive bronchiolitis and bronchitis, and destruction of parenchymal lung tissue. The most common symptoms of COPD include chronic worsening dyspnea, cough, and sputum production[1].

The Global Initiative for Chronic Lung Disease (GOLD), the world's foremost authority on COPD, recommends spirometry as the gold standard for making a definitive COPD diagnosis and considers it the most objective and reliable measure of lung function in humans. The diagnostic test measures the post-bronchodilator forced expiratory flow in 1 second ($FEV_1$) and the forced expiratory volume (FVC), following complete inspiration. Post-bronchodilator measurements are used to ensure that any observed airway narrowing is fixed; consistent with COPD pathophysiology whereas resolution of airway narrowing following bronchodilators aligns more closely with asthma pathophysiology. Chronic obstructive pulmonary disease is defined by an $FEV_1$/FVC of <0.7 and severity is classified using $FEV_1$ percent of predicted value (based on age, sex, height, and race), as described in **Table I**.

**Table I** GOLD spirometric criteria for COPD severity

| Stage | Severity | $FEV_1$/FVC | $FEV_1$ (% predicted) | Characteristics |
|---|---|---|---|---|
| 0 | At risk | >0.7 | ≥80% | Normal spirometry, chronic symptoms (productive cough) |
| I | Mild | <0.7 | ≥80% | With or without symptoms |
| II | Moderate | <0.7 | 50-80% | Symptoms progress, often include dyspnea on exertion |
| III | Severe | <0.7 | 30-50% | Symptoms worsen to limit activities of daily living; exacerbations occur |
| IV | Very severe | <0.7 | <30% or <50% plus chronic respiratory failure | Very poor quality of life; exacerbations may be life-threatening |

*Adapted from[32]

The focus of this thesis research will be on emphysema, a component of COPD that primarily manifests in patients with GOLD stage III and IV and is defined by progressive and irremediable loss of parenchymal lung tissue. The destruction of this tissue, including alveolar epithelium, capillary endothelium, and extracellular matrix components leads to decreased functional surface area, capillary blood volume, elastic recoil, and increased total lung volume. Patients with emphysema typically present with productive cough, dyspnea, and difficulty in breathing and over time can develop non-respiratory symptoms including cachexia. Because alveolar tissue is irreversibly damaged in emphysema, there is a loss of elasticity and recoil capacity allowing the lung to inflate more easily per change in pressure[33]. This increased compliance of the lung allows for hyperinflation and air trapping causing the patient to exert more effort to expel air from the lower airways, ultimately leading to fatigue and dyspnea.

*Risk Factors*

Chronic obstructive pulmonary disease has long been thought of as a "smoker's disease". While it is well accepted that cigarette smoking, whether active, passive, or secondary, is the most significant risk factor for the development of COPD, over the past decade or so, many studies in never-smokers have suggested other novel factors. These include indoor and outdoor pollution, occupational exposure to particulate matter and chemicals, poor nutrition, and early life conditions including frequent lower respiratory infections, asthma, maternal smoking, and low birth weight[34–37].

The indoor burning of biomass for cooking and heating is an increasingly appreciated factor in the growing incidence of COPD. Because biomass fuels have low combustion efficiency, a high concentration of harmful substances including carbon monoxide, formaldehyde, and benzpyrene build up while burning, making this fuel source particularly injurious to the lungs. Throughout the world, over 3 billion people are exposed to indoor burning of biomass, the

majority of whom are women and children, and about half of all COPD deaths in developing countries are attributable to biomass smoke[36].

In addition to environmental exposures, a small percentage of COPD cases can be attributed to genetic deficiencies or mutations. Approximately 1-2% of COPD patients are homozygous for the PiZ allele of the *SERPINA1* gene which is a recessive trait primarily found in Northern Europe that results in serum α-1-antitrypsin (A1AT) deficiency (the primary neutrophil elastase inhibitor) and subsequent pulmonary emphysema[38–40].

Importantly, not all patients with A1AT deficiency go on to develop emphysema and only 15-20% of smokers develop emphysema, underscoring the importance of genetic and environmental factors that play into an individual's susceptibility to the disease[41,42].

*Public health importance*

Chronic Obstructive Pulmonary Disease is associated with increased morbidity and mortality and poses a significant burden on society, the economy, and health resources world-wide. Currently, over 65 million people are living with COPD and over 90% of deaths secondary to COPD occur in low to middle income countries. Due to the chronic and progressive nature of the disease, COPD accounts for over 29 million global years lost due to disability[3] – one of the highest levels of any single disease. In the United States, medical costs for the treatment of COPD are expected to reach $49 billion by 2020 and in 2010, it's estimate that 16.4 million work days lost were attributable to COPD[43]. Due to the aging population, increasing global pollution, cigarette consumption in Asia, and indoor burning of fossil fuels in low and middle income countries, the incidence of COPD is projected to increase. In 2012, the World Health Organization ranked COPD as the third leading cause of death world-wide, representing 5.6% of global deaths, only after ischemic heart disease (13.2%) and stroke (11.9%)[2].

Despite its significant and growing public health burden, the therapy for COPD remains inadequate. Treatments are focused on limiting symptoms such as dyspnea and hypoxemia and

include the use of bronchodilators, supplemental oxygen, and glucocorticoids (effective in asthma but show little efficacy in COPD). While these therapies may help decrease the frequency and severity of exacerbations, they do nothing to limit the underlying disease processes that eventually lead to respiratory failure and death[4].

As a chronic disease that develops over time with habitual exposure to cigarette smoke and other toxic substances, the etiology of COPD and specifically emphysema, is complex. For example, while smoking is considered the greatest risk factor for developing emphysema, only a percentage of smokers end up developing the disease and a significant number of cases occur in never-smokers. It is clear that genetics and environmental exposures synergize to define an individual's susceptibility and clinical prognosis, however, the underlying mechanisms necessary to develop interventions capable of halting or slowing progression, are unknown. The overarching purpose of this thesis work is to contribute to the understanding of the immunological environment in the emphysematous lung and its role in disease progression and severity.

**Animal Models of Emphysema**

The three most common experimental animal models of emphysema are genetically-induced, cigarette smoke-induced, and protease-induced[44,45].

Certain mouse strains contain spontaneous or engineered genetic defects that result in the natural development of emphysema (reviewed in reference [44]). For example, the Pallid mouse[46] contains a nonsense mutation in Pallidin that leads to, among other phenotypic defects, serum A1AT deficiency and thus progressive emphysema beginning at one month of age. Other common strains that spontaneously develop emphysema include the osteopetrotic mouse that lacks macrophage colony stimulating factor[47], the tight skin mouse that has a duplication of fibrilin 1[48], and the blotchy mouse that has an X-linked copper transport defect[49]. Mice can also be genetically modified where a specific gene is either deleted or overexpressed to result in airspace enlargement due to alveogenesis defects, development of emphysema, or protection from the

development of emphysema after challenge with cigarette smoke or elastase. For example, deletion of surfactant protein D leads to progressive emphysema by 3 weeks of age[50] and deletion of matrix metalloprotease (MMP)-12 has been reported to protect from cigarette smoke and elastase-induced emphysema[51]. Additionally, mice lacking the epithelial integrin αvβ6 have increased expression of MMP-12 and thus develop emphysema as they age. In this model, the emphysema phenotype is averted through loss of MMP-12 or by transgenic expression of the β6 subunit that is involved in transforming growth factor-β (TGF- β)[52].

In 1990, Wright et al. demonstrated the first successful cigarette smoke induction of progressive emphysema after exposing guinea pigs to 10 unfiltered cigarettes per day, 5 days per week for up to a year in a smoking chamber[53]. The guinea pigs developed pulmonary function decline and histology similar to those of COPD patients, whereas previous models in rats and hamsters were unable to provoke diffuse progressive emphysema. The cigarette smoke model in mice produces emphysematous changes notable at 3-6 months but they are stabilized with the cessation of smoking. This is in contrast to emphysema seen in human habitual smokers where the disease usually continues to progress despite smoking cessation[44,54]. The cigarette smoke model is most useful in studies on the initiation of the disease but is costly due to the months required to produce a phenotype and is ill suited to study the progression of the disease.

The first elastolytic protease-induced model of emphysema was proposed by Gross et al. in 1965 using intratracheal administration of papain in rats[55]. Later studies found that instilling elastase (either porcine pancreatic elastase or human neutrophil elastase) into the lung was more effective at inducing the alveolar tissue destruction seen in emphysema. When a single dose of elastase is administered, it is neutralized and cleared from the lungs within 24 hours[56]. However, alveolar tissue destruction continues for weeks beyond the initial insult which is suggested to be due to the release of proteases by immune cells, such as macrophage elastase (MMP-12)[56]. Importantly, in contrast to the cigarette-smoke model which takes months to show a modest

phenotype, instillation of 3 enzymatic units (U) of elastase produces significant emphysematous changes by just one week. Recent work from Mitzner and colleagues demonstrated a strain-dependent effect of the model[57]. Whereas C57BL/6J mice show moderate emphysematous changes on stereological and pulmonary function analysis with 3U of elastase, BALB/cJ mice show significantly more pronounced damage. For instance, at 96 days post administration of 3U of elastase, BALB/cJ mice exhibited a 100% increase in total lung capacity (TLC) whereas C57BL/6J mice showed only a 20% increase in TLC compared to control mice. Due to its ability to rapidly induce progressive emphysema with a single treatment, we employ the elastase-induced emphysema model to study the progression of the disease in BALB/cJ mice.

*Evaluation of lung structure and function in animal models*

In laboratory animals, emphysema is evaluated by pulmonary function tests and lung histology. To determine the gas exchange capacity of the emphysematous lung, the diffusion factor for carbon monoxide ($DF_{CO}$), analogous to the diffusion capacity of the lungs for carbon monoxide ($DL_{CO}$) used in humans, is employed. The measurement is calculated based on the net loss of CO after a 9 second breath hold (representing the amount of CO that diffuses into the blood) compared to the dilution of a tracer gas (representing the lung volume). Values for $DF_{CO}$ range from 0 (no uptake of CO) to 1 (complete uptake of CO) and in BALB/cJ mice with elastase-induced

emphysema, are approximately decreased by 9% compared to healthy controls (**Table II**).

**Table II** Pulmonary function measures used to assess emphysema progression in elastase model

| Test | Quantifies | Healthy value* | Emphysema value† | % Change upon emphysem | Physiological significance |
|---|---|---|---|---|---|
| Total lung capacity (TLC) | Maximal inflation at 35 $cmH_2O$ [mL] | 1.378 mL ± 0.04391 | 1.791 mL ± 0.05326 | ~30% ↑ | Hyperinflation, "barrel chest" |
| Static compliance | Change in volume for any given applied pressure (3-8 $cmH_2O$) [$mL/cmH_2O$] | 0.08520 mL/H2O ± 0.003820 | 0.09528 mL/cmH2O ± 0.002366 | ~12% ↑ | Loss of alveolar and elastic tissue leads to loss of recoil and labored breathing |
| Residual volume (RV) | Trapped air volume after airway collapse on deflation [mL] | 0.1615 mL ± 0.02626 | 0.2924 mL ± 0.03347 | ~81% ↑ | Incomplete expiration due to decreased elastic recoil traps air in lungs |
| Diffusing factor of carbon monoxide ($Df_{co}$) | Transfer of gas molecules from the air to the blood; 1=complete uptake of all CO; 0=no uptake of CO | 0.7652 ± 0.01096 | 0.6965 ± 0.01190 | ~9% ↓ | Poor conductance of gas across epithelial layer due to tissue damage |

*mean ± standard error; measurements performed at day 21 in BALB/cJ mice who received 50 µL of PBS IT on day 0
† mean ± standard error; measurements performed at day 21 in BALB/cJ mice who received 3U elastase in 50 µL sterile PBS IT on day 0

To assess the mechanical functioning of the lung *in vivo*, multiple measurements can be collected using a flexiVent™ ventilator (Scireq, Montreal, QC)[58]. For example, using the single frequency forced oscillation technique (FOT), the pressure, flow, and volume values can be fit to the single compartment model to calculate the resistance, elastance, and compliance of the lung. With the low-frequency FOT, values are fit to the Constant Phase Model[59] and the input impedance, Newtonian resistance, tissue damping, and tissue elastance are calculated. To obtain quasi-static mechanical measurements, pressure-volume (P-V) loops are captured and from them the quasi-static compliance, total lung capacity, and residual volume are calculated. For our purposes, lung mechanical function changes in our mice are evaluated using the total lung capacity, residual volume, and quasi-static compliance. Average values of these measures for healthy and emphysema mice are summarized in **Table II**.

## Pathogenesis of COPD/emphysema

Over the past six decades, many environmental factors, genes, cell types, and molecular mediators have been identified for their involvement in the multifaceted pathogenesis of COPD/emphysema. However, there remains a great paucity in the understanding of how these

events and factors interact to determine individual susceptibility to developing emphysema and what mediators propagate alveolar destruction in the progressive form of the disease.

Emphysema is considered an immunological disorder with innate immune mechanisms playing a major role in the pathogenesis and progression of the disease. While some research has suggested a role for the adaptive immune system in the clinical severity of emphysema[60], experiments in severe combined immunodeficiency mice have demonstrated no difference in the phenotype of cigarette smoke-induced emphysema compared to wild type controls[61], suggesting the adaptive immune response is not crucial to the pathogenesis of emphysema.

The current paradigm for the development of COPD/emphysema is that tobacco smoke and other noxious agents initially damage and stress alveolar epithelial cells and extracellular matrix leading to the degradation of tissue components and release of DAMPs [62–64]. These danger signals then activated alveolar epithelial cells and lung macrophages to produce innate and inflammatory cytokines including TNFα, IL-1β, and IL-8[65,66]. The release of IL-1β activates alveolar macrophages and signals them to release the neutrophil chemotactic factor, IL-8. The repeated damage to the lung experienced with each inhalation of smoke or particulate matter results in ongoing recruitment of inflammatory cells including neutrophils, monocytes, and dendritic cells to the lung. When these cells arrive to the damaged tissue, they release proteases and reactive oxygen species in order to control the perceived threat and destroy foreign materials. In an acute injury or infection, these damaging molecules are usually kept in balance by anti-proteases and anti-oxidants, however, in this state of repetitive damage, regulation is lost and the initial pro-inflammatory response to injury results in a positive feedback loop and dysregulated repair process.

The aberrant immunological processes that occur during repeated exposure to noxious factors results in an imbalance of protease/anti-protease activity, oxidant/anti-oxidant activity, and lung structure maintenance components.

*Protease/anti-protease imbalance hypothesis*

In the early 1960s, researchers identified that a genetic deficiency in the serum protease A1AT led to severe early-onset emphysema[40]. Around the same time, Gross et al. proposed the first protease-induced emphysema animal model via the instillation of papain in rat lungs; together these findings led to the protease-anti-protease imbalance hypothesis of emphysema pathogenesis[67]. Innate immune cells activated in response to repeated lung injury release a variety of proteases including neutrophil elastase, matrix metalloproteases (MMP), cathepsins, collagenases, and caspases that are intended to aid in the clearance of damaged tissue, wound healing, fibrotic development, and angiogenic remodeling[68–71]. Studies of human samples of bronchoalveolar lavage (BAL) fluid and sputum have demonstrated increased expression and activity of several extracellular matrix degrading MMPs including MMP-1, MMP-8, MMP-9, and decreased expression of the anti-proteases tissue inhibitor of metalloproteases (TIMP) 1 and 2 in COPD patients compared to controls[72–74]. Additionally, many animal models of emphysema have demonstrated amelioration of the phenotype with administration of anti-proteases or loss of MMPs[51,52,75].

*Oxidant/anti-oxidant imbalance hypothesis*

The release of reactive oxygen species (ROS) from activated neutrophils, macrophages, and alveolar epithelial cells is an integral part of the innate immune response that is tightly controlled by anti-oxidants due to the damaging nature of these molecules. However, in dysregulated inflammatory states like emphysema, an imbalance in the amount of ROS relative to neutralizing species leads to tissue destruction and propagation of inflammation. For instance, upon phagocytosis of inhaled particulate matter in cigarette smoke, activated alveolar macrophages trigger the nicotinamide adenine dinucleotide phosphase (NADPH) oxidase complex and generate copious amounts of the superoxide anion which is then converted to hydrogen peroxide either spontaneously or via superoxide dismutases. The superoxide anion and hydrogen

peroxide then go on to interact with other molecules and form free radicals that exert a cytotoxic effect[76]. Similar to proteases, uncontrolled production or accumulation of oxidants is detrimental to organ structure and function, thus balance must be kept. To that end, the lungs of COPD patients contain significantly less superoxide dismutase than those of healthy controls[77] and mice lacking the nuclear erythroid-related factor 2 (Nrf-2), an antioxidant transcription factor, are sensitive to cigarette smoke exposure; developing enlarged airways, increased inflammatory response, and apoptosis of epithelial and endothelial cells[78].

*Lung structure maintenance imbalance hypothesis*

Following the initial damage to the lung caused by some noxious exposure, inflammation and tissue repair responses are initiated in an effort to restore normal lung structure and function. These repair processes include the release of growth factors (e.g. vascular endothelial growth factor [VEGF] and hepatocyte growth factor [HGF]), deposition of extracellular matrix proteins, and remodeling of the extracellular matrix[79–82].

One of the most important cell types in the tissue repair process is the fibroblast. In order to repair the parenchymal tissue damaged by cigarette smoke components and proteases released from inflammatory cells, fibroblasts are recruited to the injured site, differentiate into myofibroblasts, and synthesize protein components of the extracellular matrix as well as growth factors that stimulate alveolar epithelial cell proliferation[79], endothelial cell survival, and angiogenesis[80]. Data from human studies have demonstrated that the lung fibroblasts from emphysema patients have an altered functional capacity including reduced proliferative capability[81,83,84], increased frequency of senescence[82], reduced production of hepatocyte growth factor and functional keratinocyte growth factor[85], and decreased responsiveness to TGF-β1[86] compared to healthy control patients.

*Innate immune system*

Previous research in our laboratory has evaluated the role of neutrophils in the pathogenesis and progression of emphysema as neutrophils are elevated in the BAL fluid and sputum of COPD patients, correlate with disease severity[87], and produce many of the proteases and oxidants implicated in the disease[88]. However, long term depletion of neutrophils in elastase-treated mice had no effect on the lung histology or pulmonary function compared to neutrophil-intact controls. While neutrophils likely still play some role in the complex mechanisms of initiation and progression of disease, they do not appear essential in this model thus this work will focus on the role of macrophages in emphysema progression.

The implication of macrophages in the progression of emphysema stems from the finding that the lungs of emphysema patients have 5-10 fold more macrophages than healthy controls and that similar to neutrophils, this correlates with disease severity[89]. Further, macrophages secrete many effector molecules that can directly destroy extracellular matrix (e.g. MMP-9 and 12) or propagate inflammation (e.g. IL-8, IL-1β, IL-6, and TNF-α) [51,90,91]. Unlike neutrophils, alveolar macrophages are long-lived self-renewing cells in abundance at baseline who orchestrate the alveolar cellular milieu, a role that could easily become pathogenic in a dysregulated state.

Because tissue resident macrophages are integral to normal tissue homeostasis and monocytes can differentiate into macrophages, these populations have been investigated for their role in wound healing. In response to tissue injury, macrophages initially phagocytize apoptotic cells and debris, release proteases including macrophage elastase, and secrete chemokines to recruit other inflammatory cells to the injured tissue. Following the initial inflammation, macrophages undertake a tissue repair phenotype that includes the release of growth factors and cytokines to recruit cells such as fibroblasts and to induce local proliferation, differentiation, and angiogenesis[92]. At this point in the repair process, macrophages acquire an anti-inflammatory phenotype and are responsive to immune dampening cytokines including IL-10 and secrete both IL-10 and TGF-β1[25,93]. Interestingly, depending on the nature of injury (sterile or infectious) and

organ site, tissue resident macrophages or recruited monocytes play distinct roles in the pathogenesis of diseases of sterile inflammation and dysregulated wound repair such as athlerosclerosis[92,94], myocardial infarction[95], arthritis[96], and emphysema[68,97,98].

Recent work from our lab found that BALB/cJ mice, a strain that is highly susceptible to elastase-induced emphysema, had elevated numbers of macrophages with a mixed classically (M1) and alternatively (M2) activated phenotype (i.e. expression of inducible nitrous oxide [*inos*], arginase 1 [*arg1*], found in inflammatory zone 1 [*fizz1*]), compared to resistant C57BL/6J mice. Notably, the expression of M2-associated genes in BALB/cJ mice was elevated for a prolonged amount of time. The M2 phenotype is associated with wound healing, tissue remodeling, and the resolution of inflammation and to this end includes the secretion of extracellular matrix remodeling proteins including MMP-2, MMP-9, and MMP-12 whose expression is strongly correlated with emphysema in humans and laboratory animals[52,69,72,75].

We hypothesize that in the elastase model of emphysema, the acute injury that occurs immediately following elastase administration creates an inflammatory environment that includes the release of DAMPs such as IL-33[99,100], that act either directly or indirectly on lung macrophages to push them toward an altered repair phenotype. If lung macrophages truly are essential for the progression of emphysema, there is hope that targeted reprogramming of these cells could halt the progression of disease. Important for the development of a protocol to reprogram lung macrophages will be an understanding of the origin of these pathogenic cells.

## Specific aims

The overall goal of this thesis is to determine the cellular dynamics of resident and recruited macrophages, monocytes, and neutrophils and the role of resident macrophages in the elastase-induced emphysema model in BALB/cJ mice.

### Aim 1

***Elucidate the dynamics of resident and recruited macrophages, monocytes, and neutrophils in the lung following administration of elastase in BALB/cJ mice.***

### Aim 2

***Determine if the depletion of resident lung macrophages ameliorates or worsens elastase-induced emphysematous changes in the lungs of BALB/cJ mice.***

# MATERIALS AND METHODS

## Animals

Male wild-type (WT) BALB/cJ mice were either purchased directly from The Jackson Laboratory at 4-6 weeks of age (Stock No. 000651, Bar Harbor, ME) or bred in-house from mice originally purchased from The Jackson Laboratory. Male CD11c-DTR BALB/cJ mice, originally purchased from The Jackson Laboratory, were bred in-house (Stock No. 004509, Bar Harbor, ME). All mice used in experiments were male and 6-9 weeks of age and housed under specific pathogen-free conditions at the Johns Hopkins Bloomberg School of Public Health and were used in accordance with the National Research Council's Guide for the Care and Use of Laboratory Animals federal guidelines and the procedures were approved by the Johns Hopkins University Animal Care and Use Committee institutional review committee (Protocol number MO12H473 and MO15H461). Mice received filtered air (60-70% relative humidity) at 22-26$^0$C, were given food and water *ad libitum*, and exposed to a 12-hour light/dark cycle.

## Intratracheal elastase administration

Pulmonary emphysema was induced by administering 3U of porcine pancreatic elastase (EC-134 Elastin Products Company, Owensville, MO) via intratracheal instillation (IT). Mice were anaesthetized with a mixture of ketamine (100 mg/kg) and xylazine (15 mg/kg) via intraperitoneal injection (IP) and placed supine, suspended by their incisors using silk thread, on a 15$^0$ sloped Plexiglas platform. The neck area was treated with 70% ethanol and a 3 mm midline incision was made in the skin to expose the trachea. The tongue was gently pulled forward and to the side while a 20-gauge catheter (Jelco Optiva®, Smith Medical, Dublin, OH) with a manually bent tip was inserted toward the ventral surface of the mouse. Tracheal insertion was confirmed by visualizing the white catheter tip through the midline incision. A 3U dose of elastase suspended in 50 µL of sterile 1X phosphate-buffered saline (PBS) was instilled via the inserted catheter. To

ensure the solution was evenly distributed throughout the lungs, the mice were immediately ventilated through the catheter for 15 seconds with room air at 0.1 mL tidal volume and 250 strokes/minute using a MicroVent Ventilator (Model 848, Harvard Apparatus, Holliston, MA). Mice were monitored and allowed to recover for at least 2 days prior to evaluation at various time points post-elastase administration, as described in each experiment.

### *In vivo* labeling of resident alveolar macrophages

PKH26-PCL (PKH26PCL-1KT, Sigma-Aldrich, St. Louis, MO) is a red-fluorescent dye that is selectively taken up by phagocytic cells due to its formation of dye aggregates. A dose of 2.5 μM PKH26-PCL in 50 μL of sterile 1X PBS was administered IT, as described above, 24-48 hours prior to elastase challenge.

### Lung macrophage depletion

A 100 μL dose of either clodronate (5mg/mL)-loaded liposomes (CLL) or PBS-loaded liposomes (PLL) suspended in sterile PBS were administered IT on days 3, 5, and 7 following elastase administration. To monitor depletion efficacy, a subset of mice were sacrificed 24 hours after each liposome treatment and at days 10 and 14 following elastase. Liposomes were purchased from Dr. Nico van Rooijen (Amsterdam, The Netherlands) and are formulated as previously described[101].

### Flow cytometry

After mice were anaesthetized with Avertin (2,2,2-tribromoethanol)the lungs were removed, and the large airways were dissected away from the peripheral lung tissue. Due to the leaky nature of blood vessels during acute inflammation following elastase administration, lungs were not perfused prior to removal in order to conserve the integrity of the alveolar and interstitial cells. Excised lungs were placed in 5 mL RPMI 1640 containing 1 mg/mL collagenase type II (1701-015, Thermo Fisher Scientific, Waltham, MA) and 30 μg/mL DNase I (10104159001,

Roche Applied Science, Indianapolis, IN), minced, and incubated at $37^0$C, 5% $CO_2$ for 30 minutes. Following digestion, lung tissue was ground through a 100 μM nylon cell strainer (352360, Thermo Fisher Scientific, Waltham, MA) using a syringe plunger to form a single-cell suspension. Cells were pelleted at 1500 g at $4^0$C for 6 minutes and suspended in ACK lysis buffer (118-156-721, Quality Biological Inc., Gaithersburg, MD) at room temperature for 5 minutes to lyse any red blood cells. Cells were washed in 1X PBS, strained through a 70 μM nylon cell strainer (352350, Thermo Fisher Scientific, Waltham, MA), and pelleted at 1500 g at $4^0$C for 6 minutes, and suspended in 1X PBS. Cells were counted on a hemocytometer and approximately 1 x $10^6$ cells were stained in 1 mL of 1X PBS with LIVE/DEAD® Fixable Aqua Dead Cell viability dye (L34957, Thermo Fisher Scientific, Waltham, MA) for 30 minutes on ice in the dark. Cells were then washed in FACS buffer [1X PBS with 2% heated-inactivated fetal calf serum (35-011-CV, Mediatech, Inc., Manassas, VA)] and suspended in 100 μL FACS buffer. Because the high-affinity Fc receptor CD64 can non-specifically bind the Fc portion of other antibodies including anti-mouse CD16/CD32 Fc block (553142, BD Biosciences, San Jose, CA), cells were stained separately with CD64 for 25 minutes on ice in the dark. After washing with FACS buffer and suspending in 100 μL of FACS buffer, cells were incubated with anti-mouse CD16/32 Fc block for 10 minutes, and stained with the remaining antibody panel for 25 minutes on ice in the dark.

All samples were collected on a BD LSR II flow cytometer using BD FACSDiva software (BD Biosciences, Franklin Lakes, NJ). The LSR II configuration and voltages used to collect all samples are displayed in **Figure 4** and **Table III**, respectively. All antibodies used are listed in **Table IV**.

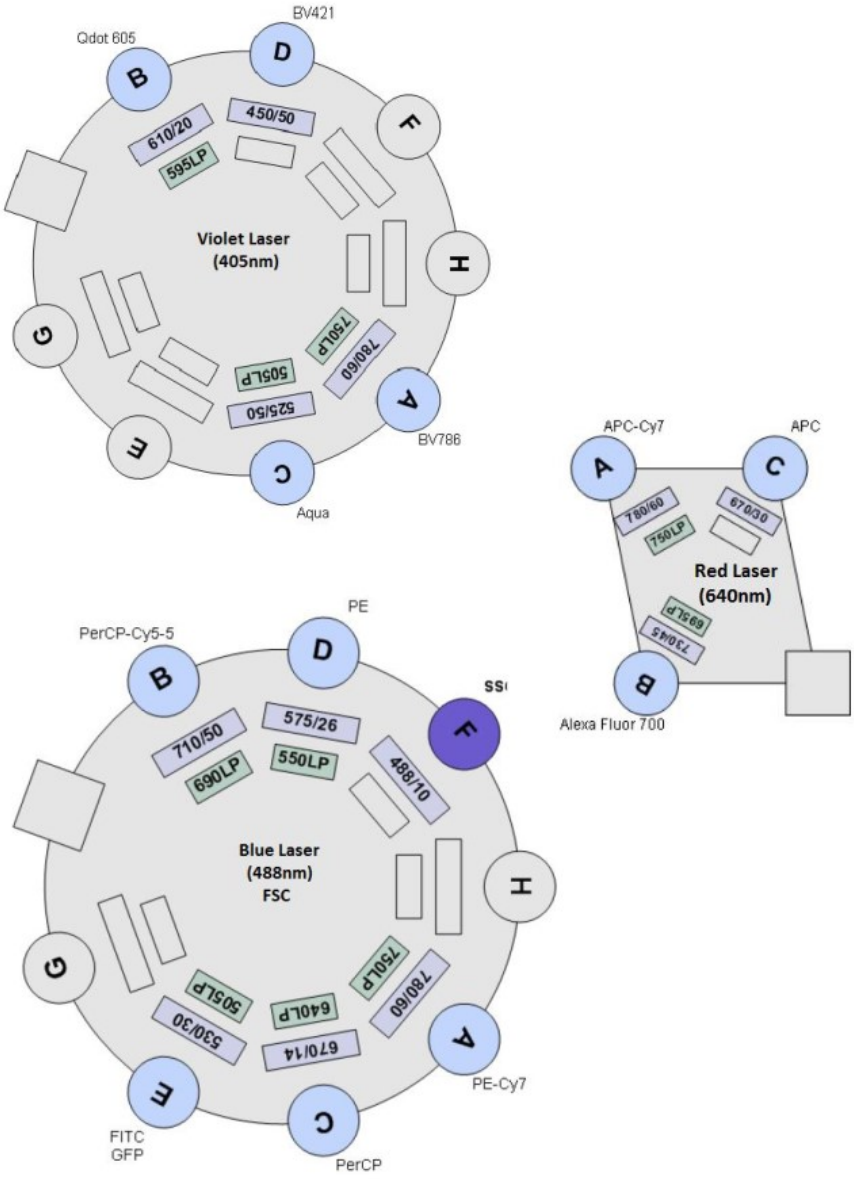


**FIGURE 4 BD Bioscience LSR II flow cytometer configuration**

| **Table II** BD LSR II settings | |
|---|---|
| **Parameter** | **Voltage** |
| FSC | 325 |
| SSC | 372 |
| Aqua | 372 |
| PE/Cy7 | 513 |
| APC/Cy7 | 499 |
| FITC | 497 |
| Alexa Fluor 700 | 479 |
| BV605 | 430 |
| BV785 | 483 |
| BV421 | 338 |
| APC | 532 |
| PE | 405 |

**Table IV** Flow cytometry antibody panel for detection of myeloid cell subsets in the murine lung

| Antigen | Fluorophore | Clone | Vendor | Catalog No. | Dilution |
|---|---|---|---|---|---|
| **LIVE/DEAD™** | Aqua | | ThermoFisher Scientific | L34957 | 1:1000 |
| **CD64** | PE/Cy7 | X54-5/7.1 | BioLegend | 139314 | 1:50 |
| **CD45** | APC/Cy7 | 30-F11 | BioLegend | 103116 | 1:200 |
| **Ly6C** | FITC | HK1.4 | BioLegend | 128005 | 1:200 |
| **Ly6G** | Alexa Fluor 700 | 1A8 | BioLegend | 127621 | 1:200 |
| **I-A/I-E** | BV605 | M5/114.15.2 | BioLegend | 107639 | 1:200 |
| **CD11b** | BV785 | M1/70 | BioLegend | 101243 | 1:100 |
| **SiglecF** | BV421 | E50-2440 | BD Biosciences | 562681 | 1:133 |
| **CD11c** | APC | N418 | Miltenyi Biotec | 130-102-493 | 1:33 |

**Flow cytometry analysis**

All data was analyzed using FlowJo software (TreeStar, Inc., Ashland, OR). Because the total number of cells changes over the course of inflammation and emphysema progression, quantifying cell dynamics by directly using the flow cytometry data output of percentage of a certain population can introduce bias therefore, cells per lung were quantified in the following manner. The percentage of live, singlet cells was calculated by first gating on "cells" using forward scatter area (FSC-A) and side scatter area (SSC-A) to exclude red blood cells and debris (**Figure 5**). Forward scatter height (FSC-H) and FSC-A were used to gate on singlets and from this population, live cells were identified using LIVE/DEAD® and side scatter height (SSC-H). The frequency of live, singlet, cells was applied to whole lung hemocytometer calculations to compute an approximate number of cells per lung. Notably, lungs were harvested without perfusing in order to maintain certain immune cell populations that could be lost during perfusion. However, this means that calculations reflect not only cells of lung tissue but also of the vascular space, obviously influenced by the amount of hemorrhaging. To account for spectral overlap and issues of compensation, fluorescence-minus-one (FMO) controls were used to define all gates. Once gates were defined, the gated population's percentage of live, singlet, cells was applied to the calculated whole lung cell count to derive the number of cells of the given population were in the whole lung.

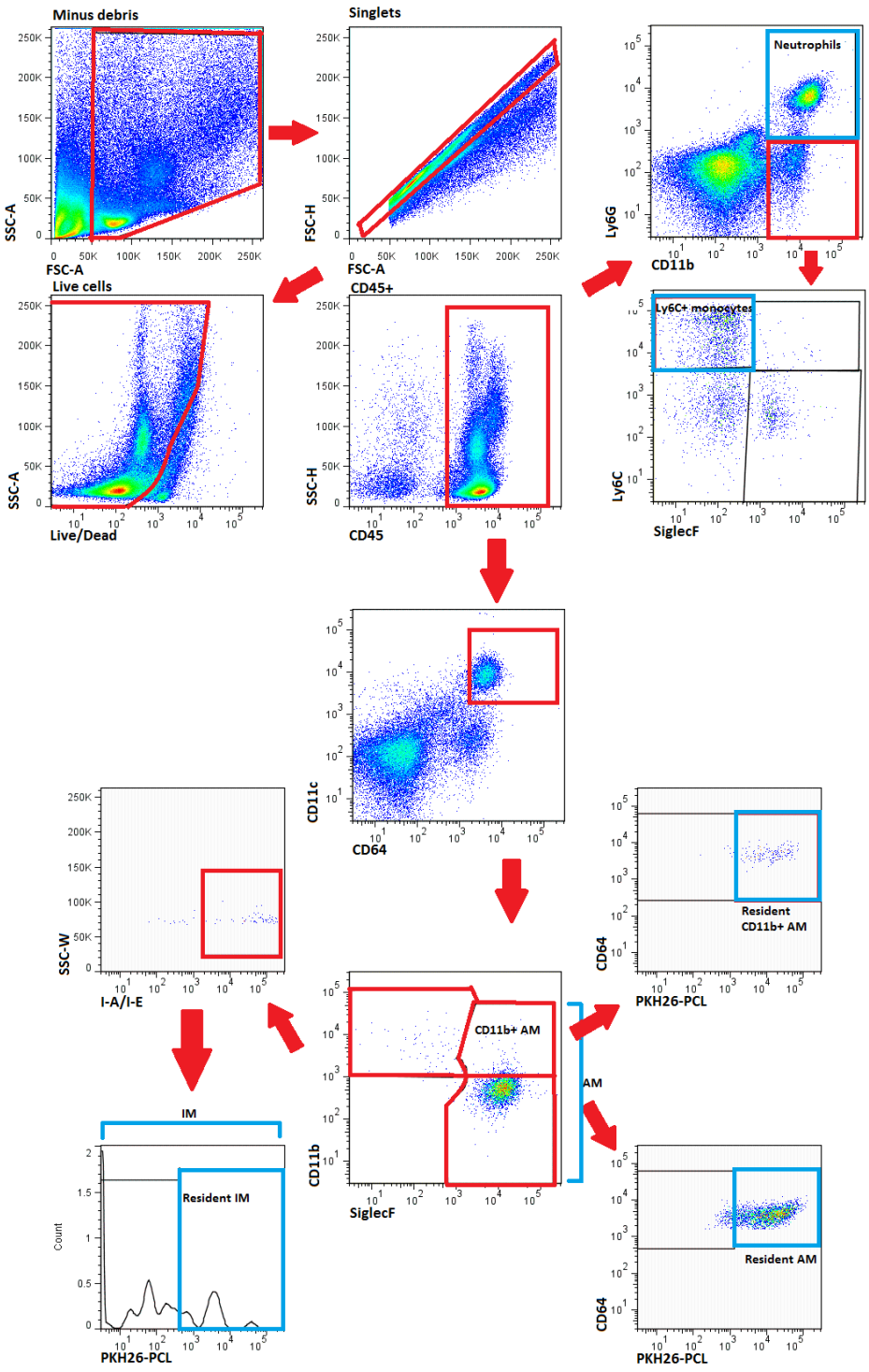


**FIGURE 5 Flow cytometry gating scheme**

**Diffusion factor for carbon monoxide ($DF_{CO}$) measurement**

Mice were anaesthetized with a mixture of ketamine (100 mg/kg) and xylazine (15 mg/kg) IP and tracheostomy was performed using an 18 G stub needle cannula. The lungs were then inflated with 0.8 mL of gas containing approximately 0.5% carbon monoxide (CO), 0.5% neon (insoluble inert tracer gas), and room air. After holding the lungs inflated for 9 seconds, 0.8 mL of gas was quickly withdrawn from the lung and diluted with 2 mL of room air to ensure all sample gas cleared the system. The exhaled gas was then injected into a Micro GC gas chromatograph (INFICON, Micro GC Model 3000A, East Syracuse, NY) to measure the concentration of Ne and CO. The process was repeated a total of three times per animal and the average Ne and CO concentrations were used to calculate the $DF_{CO}$[102].

$$1 - \frac{\frac{CO_9}{CO_C}}{\frac{Ne_9}{Ne_C}}$$

Equation for calculation of $DF_{CO}$ where "9" subscript refers to the gases after the 9 second breath hold and "C" subscript refers to the calibration gases.

**Pulmonary mechanics and quasi-static pressure-volume relationships**

Following $DF_{CO}$ measurements, mice were given an intramuscular injection of succinylcholine (75 mg/kg) to induce paralysis. They were then connected to a flexiVent™ ventilator (Scireq, Montreal, QC), providing a constant-volume ventilation of 100% oxygen at tidal volume 10 mL/kg and rate of 150 breaths per minute, with a positive end-expiratory pressure (PEEP) of 3 $cmH_2O$. After 3 minutes of ventilation, the lungs were inflated to 30 $cmH_2O$ for 5 seconds and returned to normal ventilation for 1 minute. Respiratory mechanics were measured under closed chest conditions by applying an oscillatory pressure (FOT) to the lungs and measuring flow responses to the applied pressures. Before taking the FOT measurement, conventional single-compartment mechanics were measured with 2 seconds of a 2.5 Hz sinusoidal oscillation to obtain respiratory system resistance (Rrs), dynamic compliance (Crs), and elastance

(ErS)[103]. Newtonian airway resistance (*Rn*), tissue damping (*G*), and tissue elastance (*H*) were obtained by performing the broadband FOT maneuver and analyzing the constant phase model.

Next, the lung was sealed off for 4 minutes by closing the stopcock leading to the cannula, allowing for the absorption of all gas, and resulting in a lung volume of zero. Quasi-static P-V curves were generated via a previously detailed system[104]. In brief, the system is comprised of 5 mL glass syringe filled with an initial volume of 3 mL of air, which is mounted on a dual infusion-withdrawal syringe pump (model 55-2226, Harvard Apparatus, Holliston, MA). A linear displacement transformer (model 244-000, Transtek, Ellington, CT) measures the air volume delivered to the lung and a differential-pressure transducer (PX-137, Omega Engineering, Stamford, CT) measures the airway pressure. The P-V curve generated from measured airway pressure and volume was recorded on a PowerLab digital data acquisition system (ADInstruments, Colorado Springs, CO). During the initial inflation of the degassed lung, a flow rate of 1 mL/min was employed to avoid excessive pressure. The flow rate was increased to 3 mL/min until a pressure of 35 $cmH_2O$, at which point the pump was immediately reversed to deflate the lung until obtaining a pressure of -10 $cmH_2O$. Two additional P-V loops from 0-35 $cmH_2O$ were obtained to ensure there was no obstruction or leak in the system or lung. For each mouse, total lung capacity (TLC) and residual volume (RV) were defined as the volume at 35 $cmH_2O$ and -10 $cmH_2O$, respectively. Quasi-static compliance of the respiratory system (C-stat) was defined as the slope of the most linear portion of the P-V curve (between 3 and 8 $cmH_2O$).

**Statistical Analysis**

Differences between groups were analyzed by either a two-tailed unpaired *t*-test (Student's for equal variances or Welch's for unequal variances). The threshold of significance was defined as $\alpha=0.05$. All analyses were performed using GraphPad Prism 6 (GraphPad, La Jolla, CA).

# RESULTS

## Part 1: *What are the dynamics of resident and recruited macrophages, monocytes, and neutrophils in the lung following administration of elastase in BALB/cJ mice?*

*Flow cytometry*

A 10-color flow cytometry panel was designed to distinguish alveolar macrophages, interstitial macrophages, monocytes, and neutrophils, as summarized in **Table IV**. To differentiate resident and recruited lung cells, the dye PKH26-PCL was given prior to administering elastase and was detected by flow cytometry using the PE channel. Staining alveolar macrophages with PKH26-PCL has been previously shown by our lab and others to stably label phagocytic lung cells for up to 30 days in the naïve lung. Alveolar macrophages have an extremely low proliferation rate (half-life of ~12 months) in the absences of lung injury[25]. However, given the ensuing inflammation following elastase challenge, PKH26-PCL was given in the 24-48 hour time point prior to elastase for all mice to account for any influence in the time from labeling with PKH26-PCL and elastase challenge.

The gating schematic used to identify macrophage, monocyte, and neutrophil populations is displayed in **Figure 5** and the markers used to classify each cell type are summarized in **Table V**.

**Table V** Surface antigens used in flow cytometric immunophenotyping

| ***Cell type*** | ***Antigens*** |
|---|---|
| Alveolar macrophage | $CD45^+$, $CD64^+$, $CD11c^+$, $SiglecF^+$ |
| CD11b+ alveolar macrophage | $CD45^+$, $CD64^+$, $CD11c^+$, $SiglecF^+$, $CD11b^+$ |
| Interstitial macrophage | $CD45^+$, $CD64^+$, $CD11c^+$, $SiglecF^-$, $CD11b^+$, MHC $II^+$ |
| Ly6C+ monocyte | $CD45^+$, $CD11b^+$, $Ly6G^-$, $Ly6C^+$ |
| Neutrophil | $CD45^+$, $CD11b^+$, $Ly6G^+$ |

Under steady state conditions, alveolar macrophages do not express CD11b however, previous research in our laboratory has demonstrated that alveolar macrophages upregulate

CD11b during inflammation. To this end, we decided to define alveolar macrophages by the antigens CD64, CD11c, and SiglecF and stratify this population by CD11b expression.

Based on previous data regarding the general inflammatory environment over the course of elastase-induced lung injury and subsequent emphysema, we chose to study the immune environment at 2, 4, 7, 10, and 14 days post-elastase administration. Briefly, mice were given PKH26-PCL IT between 24 and 48 hours prior to receiving 3U of elastase IT and then sacrificed for analysis by flow cytometry at the designated time points (**Figure 6**). Naïve mice were sacrificed 24-48 hours following administration of PKH26-PCL.

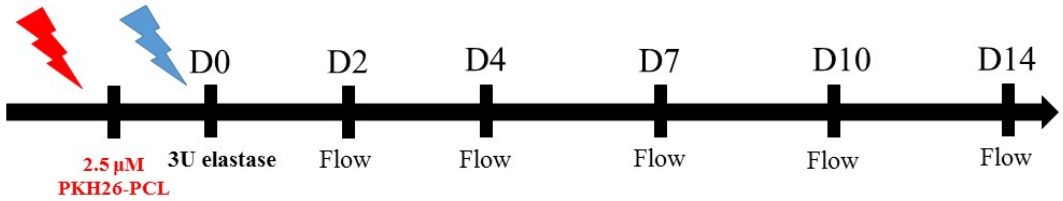


**FIGURE 6 Experimental design for elucidating dynamics of resident and recruited myeloid cells in the elastase treated lung** Mice were give 2.5 µM of PKH26-PCL dye IT 24-48 hours prior to the administration of 3U of elastase IT. D0 indicates mice that received PKH26-PCL dye and were sacrificed 24-48 hours after administration. All mice were sacrificed at the indicated time points and flow cytometric analysis was performed the same day.

*Whole lung cell count*

At baseline, male BALB/cJ mice have an average of 1 x $10^7$ cells in the unperfused lung (**Figure 7**). At two days following elastase challenge, there is significant hemorrhaging, cellular infiltration, and presumably proliferation throughout the lung resulting in the number of cells doubling. The cellular expansion peaked at day 4 and by day 7 much of the hemorrhaging had subsided and lung cell numbers decline to around 1.4 x $10^7$ cells per lung at day 14 post-elastase. The response between days 0 and 4 is reflective of the acute injury phase of elastase-induced inflammation with resolution of the hemorrhaging and cellular infiltration occurring from day 7 onward.

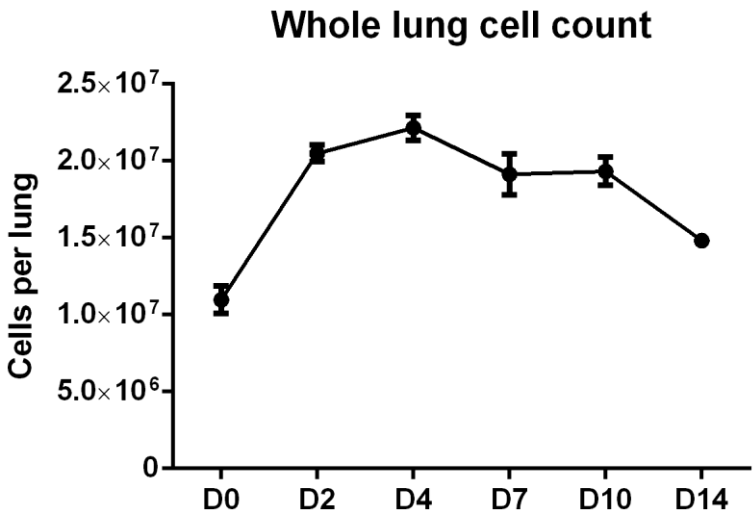


**FIGURE 7 Whole lung cell count following elastase administration** Whole lung cell counts were derived by applying flow cytometry gating calculations of the percentage of collected cells that were live and singlet, to hemocytometer counts of cells. Each point represents the mean ± standard error of the mean (SEM) with an average of 9 mice per time point.

*PKH26-PCL⁺ cells*

In preliminary studies, the optimal concentration of PKH26-PCL, 2.5 μM, was determined by titrating the dose of dye and analyzing by flow cytometry to achieve a clear positive shift on flow cytometry. The overwhelming majority of PKH26-PCL⁺ cells were alveolar or interstitial macrophages, non-phagocytic cells such as epithelial calls and fibroblasts were PKH26-PCL (data not shown). We aimed for a conservative concentration of dye to avoid the possibility of excess dye exiting the lung and staining peripheral phagocytes or staining infiltrating phagocytes following elastase administration.

While PKH26-PCL+ cells included both alveolar and interstitial macrophages, a majority of the labeled cells had a surface phenotype of alveolar macrophages. The reason for the lower number of labeled interstitial macrophages is unclear but the less efficient labeling may have been due to their spatial location and reduced access to the dye. The percentages of alveolar macrophages, interstitial macrophages, neutrophils, and monocytes that were PKH26-PCL⁺ are displayed in **Figure 8**. Importantly, the percentage of monocytes that were PKH26-PCL⁺ was

exceedingly low at all time points. In the naïve lung, less than 2% of the PKH26-PCL$^{+}$ were neutrophisl, however, this increased to almost 8% on day 7 post-elastase and subsequently declined to less than 4% by day 10. Upon analyzing these PKH26-PCL populations by SSC-A and FSC-A, it appears they are macrophages that are either ending up in the neutrophil gate due to the gating strategy applied or they are macrophages that efferocytosed neutrophils and gained Ly6G expression via trogocytosis[105]. Overall, the utilization of PKH26-PCL dye appears to be a reliable method to label the vast majority of macrophages in the alveolar space and to a lesser extent in the interstitial spaces.

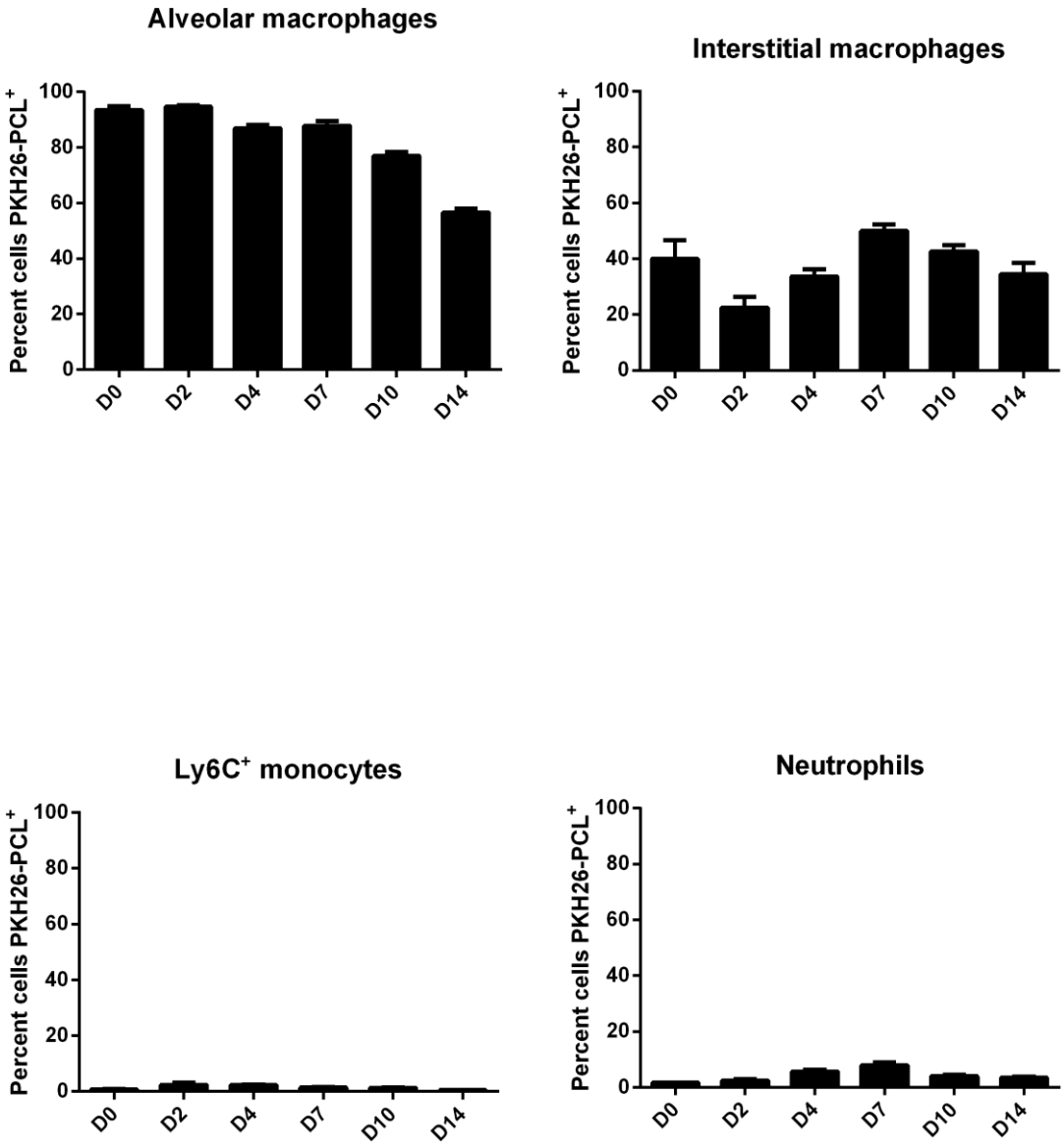


**FIGURE 8 Efficacy of PKH26-PCL labeling of resident lung cells** Data are presented as the percentage of a given cell type (e.g. alveolar macrophages) that are PKH26-PCL$^+$ as analyzed by flow cytometry. *Alveolar macrophages* are defined as CD64$^+$, CD11c$^+$, SiglecF$^+$ and on average 94% are PKH26-PCL$^+$ at D0 and D2, 85% are PKH26-PCL$^+$ at D4 and D7, and 76% and 56% are PKH26-PCL$^+$ on D10 and D14, respectively. *Interstitial macrophages* are defined as CD64$^+$, CD11c$^+$, SiglecF$^-$, CD11b$^+$, MHCII$^+$ and on average 40% are PKH26-PCL$^+$ on D0, 22% are PKH26-PCL$^+$ on D2, 33% are PKH26-PCL$^+$ on D4 and D14, and 45% are PKH26-PCL$^+$ on D7 and D10. Of *Ly6C$^+$ monocytes* ≤2% are PKH26-PCL$^+$ at all time points. Of *Neutrophils* ≤2% are PKH26-PCL$^+$ at D0 and D2, 5.5% are PKH26-PCL$^+$ at D4, 7.8% are PKH26-PCL$^+$ at D7, and 3.5% are PKH26-PCL$^+$ at D10 and D14. Each bar represents the mean ± SEM with an average of 9 mice per time point.

*Alveolar macrophages*

The alveolar macrophage population fluctuates over the course of the inflammatory response to elastase-induced damage with a return to a near-baseline level around day 14, which is consistent with other lung injury models[25,106]. From the time of elastase administration until day 4 post-elastase, there is a 2.6-fold contraction of the alveolar macrophage population (**Figure 9A, black line**). Between days 4 and 10 post-elastase, that population doubles and is followed by a subsequent decline out to day 14.

After the administration of elastase, a subpopulation of resident alveolar macrophages upregulates CD11b surface expression. This population almost doubles by day 2 post-elastase (**Figure 9A, blue line**). By day 7, the population reaches over 5 times that of the naïve lung. Between days 7 and 10, the $CD11b^+$ resident alveolar macrophage population either contracts through apoptosis, migration to the draining lymph nodes, or downregulation of CD11b, reaching a population close to baseline by day 14.

Stratifying alveolar macrophages by PKH26-PCL staining to identify resident cells (**Figure 9B**) demonstrates that the overall alveolar macrophage population dynamics are primarily attributable to resident cells while a small population of $PKH26\text{-}PCL^-$ alveolar macrophages emerges around day 4 when it more than doubles and continues to increase through day 14 post-elastase.

Overall, the expansion of alveolar macrophages in the lung between days 7 and 10 post-elastase appears to be primarily attributable to local cell proliferation as there is an increase in the number of $PKH26\text{-}PCL^+$ cells. Additionally, there is a subpopulation of alveolar macrophages that upregulate the expression of CD11b suggesting that as the cells expand there are changes in their activation status.

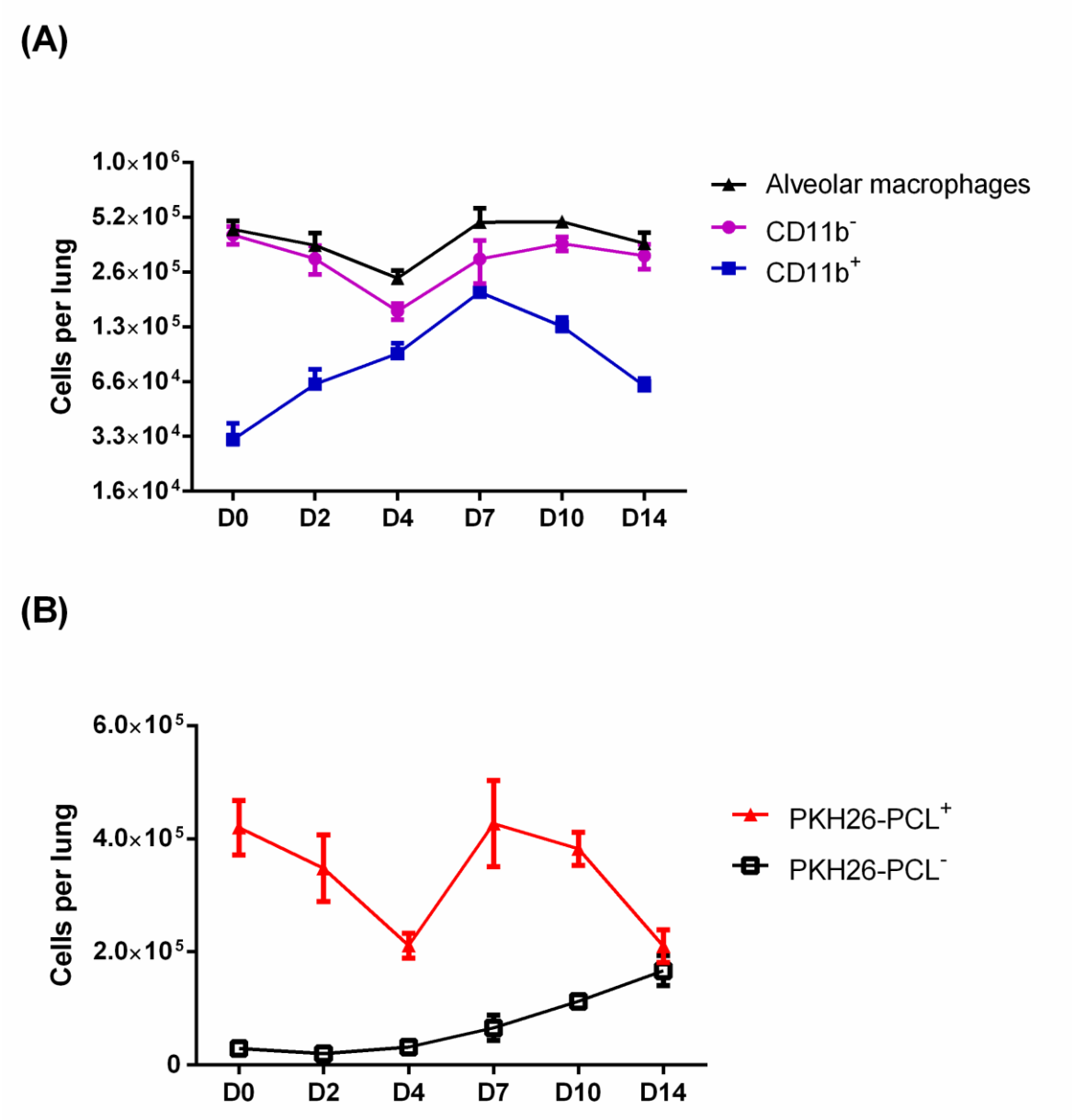


**FIGURE 9 Alveolar macrophage dynamics in the lung following elastase administration**
Alveolar macrophages are defined as CD64⁺, CD11c⁺, SiglecF⁺ and are stratified by (A) CD11b expression and (B) PKH26-PCL, where PKH26-PCL⁺ cells represent resident alveolar macrophages. Each point represents the mean ± SEM with an average of 9 mice per time point.

*Interstitial macrophages*

The resident interstitial macrophage population undergoes proliferation following the administration of elastase with an almost 32 fold increase from baseline by day 4 (**Figure 10**). The population then contracts to a population size approximately 6-fold higher than baseline by day

14. The PKH26-PCL$^-$ population of interstitial macrophages shows a similar dynamic, increasing over 32 fold to peak by day 4 post-elastase. By day 14 post-elastase, the PKH26-PCL$^-$ population decreases with kinetics similar to that observed for the PKH26-PCL$^+$ cells.

To facilitate the comparison of the dynamics of each macrophage population, data for the three subsets have been plotted together in **Figure 11**. Interestingly, in **Figure 8** there is a gradual but significant decline in the percentage of positive alveolar macrophages from day 7 to day 14 post-elastase. This could be due either to dilution of the dye through multiple cell divisions, proliferation of unlabeled resident alveolar macrophages, or through the differentiation of PKH26-PCL$^-$ interstitial macrophages into alveolar macrophages. **Figure 11B** shows a steady increase in the number of PKH26-PCL$^-$ alveolar macrophages from day 4 to day 14 while at the same time there is a steady decline in interstitial macrophages following their sharp peak at day 4. Further, the increase in the absolute number of PKH26-PCL$^-$ alveolar macrophages mirrors the decrease in the number of PKH26-PCL$^-$ interstitial macrophages. In support of this hypothesis is a 2007 publication by Landsman and Jung demonstrating that following alveolar macrophage depletion, interstitial macrophages proliferated and migrated into the alveolar space and were replenished by Ly6C$^-$ monocytes. Our observed Ly6C$^+$ monocytes dynamics do not appear to contribute to the PKH26-PCL$^-$ interstitial macrophage expansion so perhaps it is due to Ly6C$^-$ monocytes as the authors witnessed, or simply local proliferation of unlabeled resident interstitial macrophages. Further cell labeling experiments are needed to elucidate the exact dynamics of these macrophage populations.

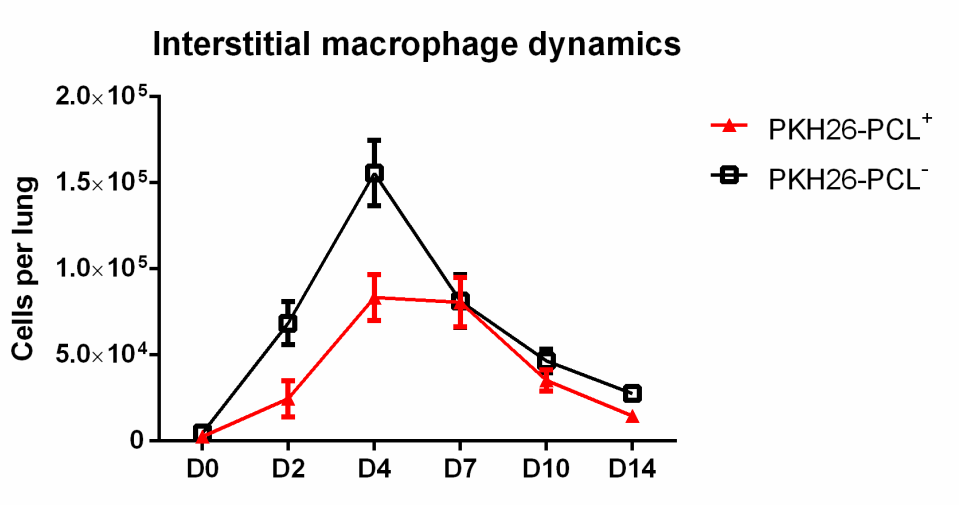


**FIGURE 10 Interstitial macrophage dynamics in the lung following elastase administration**
Interstitial lung macrophages are defined as CD64+, CD11c+, SiglecF+, CD11b+, MHCII+ and are stratified by PKH26-PCL labeling. Each point represents the mean ± SEM with an average of 9 mice per time point.

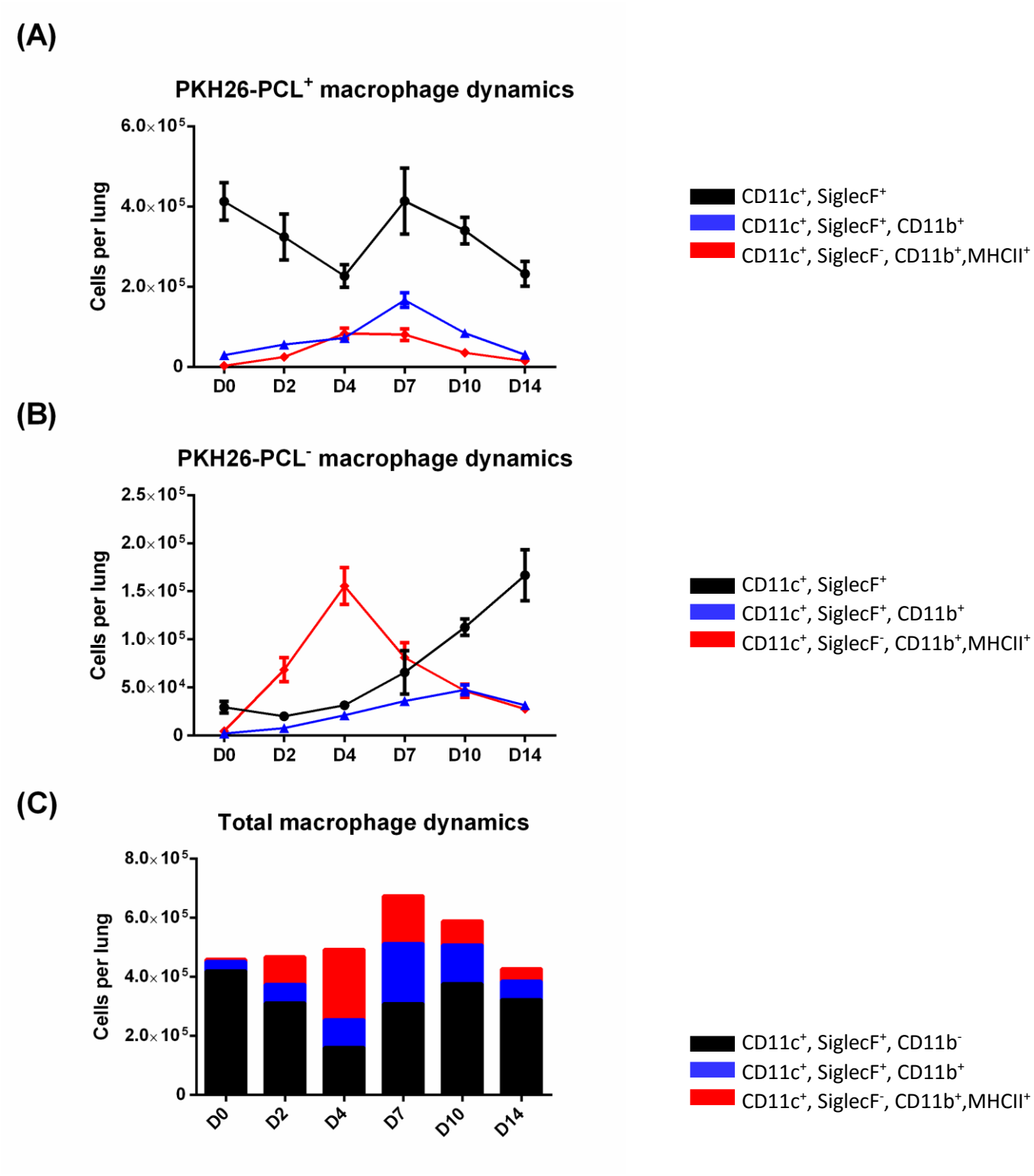


**FIGURE 11 Macrophage subset dynamics in the lung following elastase administration** (A) PKH26-PCL+ cells (B) PKH26-PCL- cells. (C) All macrophages independent of PKH26-PCL staining; alveolar macrophages are stratified by CD11b expression so that the total of the black and blue bars represents the total number of alveolar macrophages. Each point/bar represents the mean ± SEM with an average of 9 mice per time point.

*Ly6C⁺ monocytes*

The number of Ly6C⁺ monocytes in the lung more than doubles by day 2 post-elastase, which is expected due to the significant hemorrhaging and acute injury to the lung (**Figure 12**). By day 4, the number of monocytes peaks at a little under one million cells and by day 14, it returns to baseline. Interestingly, the magnitude of infiltrating monocytes is less than one might expect given the significant damage to the lung. This may be a result of the markers we employed to identify Ly6C⁺ monocytes as infiltrating cells may be altering their phenotype immediately upon entry into the lung and thus would not be captured in our panel.

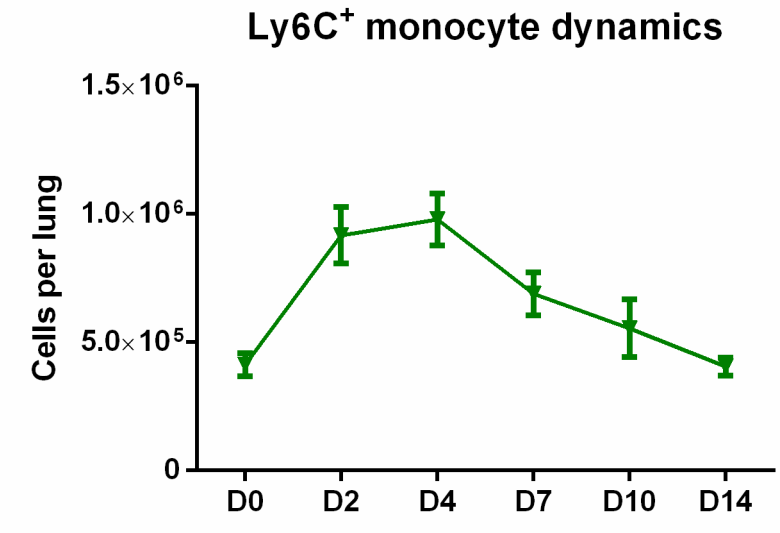


**FIGURE 12 Ly6C⁺ monocyte dynamics in the lung following elastase administration** Each point represents the mean ± SEM with an average of 9 mice per time point.

*Neutrophils*

Given the significant damage to the lung that occurs immediately following elastase administration, the rapid influx of neutrophils into the lung is expected. By day 2 post-elastase, the number of neutrophils triples and by day 4 begins to gradually decline to baseline, by day 14

(**Figure 13**). The relative dynamics of the macrophage subsets, monocytes, and neutrophils are depicted in **Figure 14**.

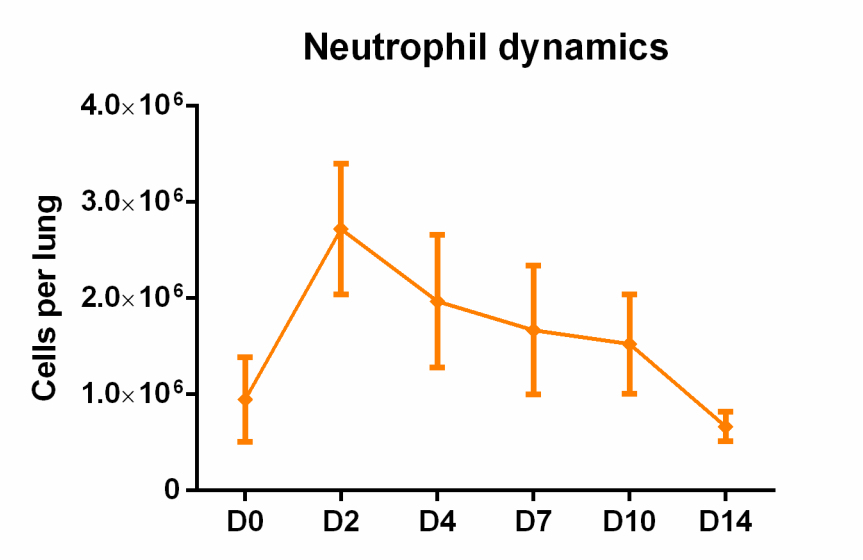


**FIGURE 13 Neutrophil dynamics in the lung following elastase administration** Each point represents the mean ± SEM with an average of 9 mice per time point.

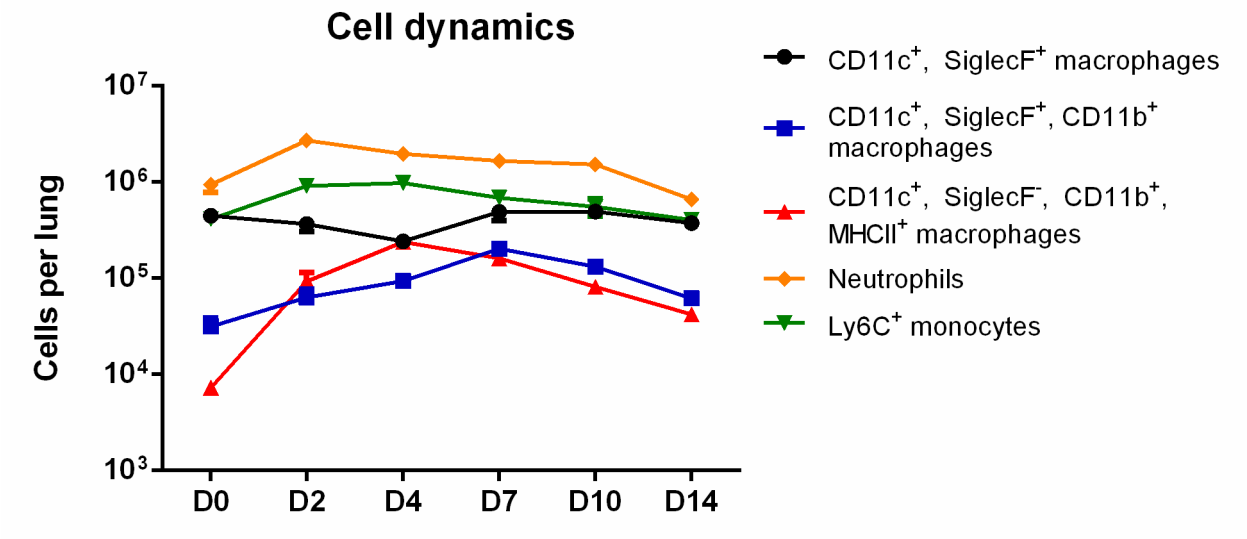


**FIGURE 14 Myeloid cell dynamics in the lung following elastase administration** Each point represents the mean ± SEM with an average of 9 mice per time point.

## Part2: *Does depletion of lung macrophages impact the cellular response and functional parameters after elastase challenge?*

*Resident macrophage depletion*

Because alveolar macrophages are long-lived cells that produce many of the effector molecules implicated in the progression of emphysema, we hypothesized that they may play a role in the progressive alveolar destruction and declining lung function following elastase administration.

Previous research in the lab attempted to delineate the importance of alveolar macrophages during the initiation and progression of elastase-induced emphysema by depleting alveolar macrophages via intratracheal aspiration of CLL or PLL 1 day prior to elastase challenge and at days 2, 7, or 14 post-elastase. Examination of histopathological sections indicated there was no difference between mice given PLL or CLL at any of the studied time points. However, while depletion efficacy was 83% when administered 1 day prior to elastase challenge, the efficacy declined to 45%, 68%, and 42% at days 2, 7, and 14 post-elastase, respectively.

We hypothesized that the poor depletion efficacy at time points following elastase administration was either secondary to a physical barrier to liposomes reaching the macrophages due to the amount of hemorrhaging and edema in the lung, or due to the animals not being able to aspirate well enough once acute lung injury and emphysema were induced. In an attempt to improve the depletion efficacy, we tested the effect of giving a second dose by administering liposomes on days 3 and 4 via intratracheal aspiration. However, the mice barely survived the first dose on day 3 and two thirds of the mice died immediately following the second dose on day 4. Because death was instant, we presumed it was due to an overwhelming amount of fluid in lungs already inundated with edema and blood, essentially drowning the mice. Due to this delicate time point, we repeated the pilot experiment, instead giving liposomes on days 4 and 5 post-elastase.

While all of the mice survived the treatments, the depletion efficacy 24 hours after the second dose was only 67%.

Due to the unsatisfactory depletion efficacy of intratracheally aspirated CLL, we decided to attempt to deplete alveolar macrophages using BALB/c CD11c-diphtheria toxin receptor (DTR) mouse model. Because mice do not normally express the diphtheria toxin receptor, transgenic mice that express the diphtheria toxin receptor in a given cell type will deplete this cell when administered diphtheria toxin. CD11c-DTX mice express the simian diphtheria toxin receptor under control of the murine *integrin alpha X* (*Itgax* – CD11c) promotor, typically expressed primarily on dendritic cells. Because alveolar macrophages express high levels of CD11c, we were able to administer diphtheria toxin directly to the lung and primarily deplete alveolar macrophages. The benefit of using diphtheria toxin over liposomes is that diphtheria toxin does not have the level of viscosity that liposomes have and can be given in a 50 μL volume as opposed to 100 μL. A series of pilot experiments were performed to evaluate the most efficient dose of diphtheria toxin in terms of depletion efficacy and animal survival as repeated doses of diphtheria toxin have proven to be lethal. We found a dose of 90 ng in 50 μL of sterile 1X PBS to best achieve this (data not shown) and gave the toxin solution via intratracheal aspiration 1 day prior to elastase challenge and on days 2, 4, and 6 post-elastase in order to ensure continued depletion of the population. Unfortunately, while we found the depletion efficacy to be between 80-89% on days -1, 2, and 6 and 45-77% efficacy on day 4, mice experienced significant weight loss and were quite ill by day 7.

Due to the mediocre depletion efficacy and illness experienced by the CD11c-DTR mice, we decided to attempt to employ CLL again. During intratracheal aspiration following elastase administration, mice noticeably have difficulty aspirating liquid and appear unable to make the effort for deep inspiration, necessary for effective liposome administration into the alveolar space. To address this issue, we explored giving the liposomes IT where the mice are intubated with a

cannula, the liposome solution is instilled via pipette, and the cannula is connected to a room-air ventilator to ensure the solution is distributed evenly throughout the lung and to give the animals supplemental air during this process. We determined that mice were able to tolerate three doses of liposomes given IT on days 3, 5, and 7 post-elastase with a depletion efficacy of 97% following the third dose. The timing of depletion was chosen based on the alveolar macrophage dynamics where we see an initial decline in cells followed by a significant proliferation peaking by day 7.

*Depletion efficacy*

**Table VI** summarizes the depletion efficacy of alveolar macrophages at 24 hours following each liposome dose and at 3 and 7 days following the third dose of liposomes (days 10 and 14 post-elastase). Mice evaluated on day 4 received 1 dose of liposomes on day 3 post-elastase, mice evaluated on day 5 received a total of 2 doses of liposomes on days 3 and 5 post-elastase, and mice evaluated on days 8, 10, and 14 received a total of 3 doses on days 3, 5, and 7 post-elastase (**Figure 15**).

**Table VI** Alveolar macrophage depletion efficacy*

| Day post-elastase | Liposome administration day(s) | Depletion efficacy, % | Depletion efficacy ($PKH26\text{-}PCL^+$), % |
|---|---|---|---|
| 4 | 3 | 85.00 | 92.69 |
| 6 | 3, 5 | 94.61 | 91.69 |
| 8 | 3, 5, 7 | 98.06 | 91.70 |
| 10 | 3, 5, 7 | 91.41 | 94.06 |
| 14 | 3, 5, 7 | 92.63 | 92.82 |

* $CD64^+$, $CD11c^+$, $SiglecF^+$ alveolar macrophages of elastase+CLL mice vs elastase only mice

Depletion of resident alveolar macrophages was maintained between approximately 92-94% from day 4 through at least day 14 post-elastase. Regarding the entire alveolar macrophage population (i.e. not taking into account PKH26-PCL labeling), the depletion efficacy was maintained between 85-98%, with the highest degree of depletion being 24 hours after the third liposome treatment.

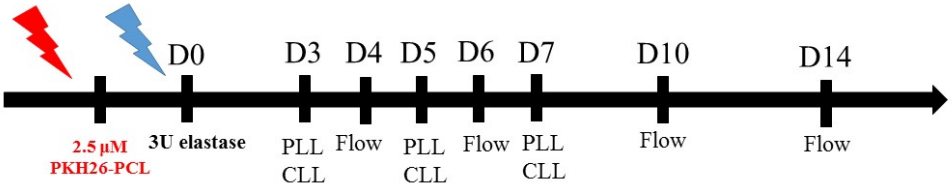


**FIGURE 15 Experimental design to evaluate clodronate-loaded liposome depletion efficacy and cellular dynamics** Mice were given 2.5µM of PKH26-PCL dye IT 24-48 hours prior to administration of 3U of elastase IT. Mice were then administered 100µL of either PLL or CLL IT as a total of one dose at D3; two doses at D3, D5; or three doses at D3, D5, D7. Mice were sacrificed and flow cytometric analysis was performed 24 hours following the last liposome treatment and at days 3 and 7 following the final D7 dose.

*Cell dynamics following macrophage depletion*

*Alveolar macrophages*

The resident alveolar macrophage ($CD64^+$, $CD11c^+$, $SiglecF^+$, $CD11b^+$, $PKH26\text{-}PCL^+$) population in mice that received elastase and CLL (E+CLL) was on the order of 11.9 x $10^3$ cells following one dose of liposomes and was 1.84 x $10^3$ cells following the third dose which remained stable at 1.8 x $10^3$ cells one week later (**Figure 16A**). This is in contrast to mice receiving elastase and PLL (E+PLL) whose resident alveolar macrophage population steadily increased from 1.5 x $10^3$ cells following a single dose of PLL until reaching 221.7 x $10^3$ cells one week following the last dose of liposomes.

Interestingly, E+PLL mice has almost an order of magnitude fewer alveolar macrophages compared to mice given elastase-only (**Figure 16B).** This population undergoes a steady expansion until day 10 when there is a doubling of cells at day 14. Conversely, in the elastase-only mice, the resident alveolar macrophage population doubles between days 4 and 7 and subsequently declines to about half the population of cells in the naïve lung, by day 14.

Similar to the results from Aim 1, a subpopulation of alveolar macrophages in the elastase+liposome model upregulate CD11b expression. However, in E+CLL mice, the population of resident $CD11b^{+}$ alveolar macrophages is quite small and fairly constant between days 4 and 14 post-elastase (data not shown). In mice receiving E+PLL, the CD11b expression dynamics are similar to those of elastase-only mice.

16

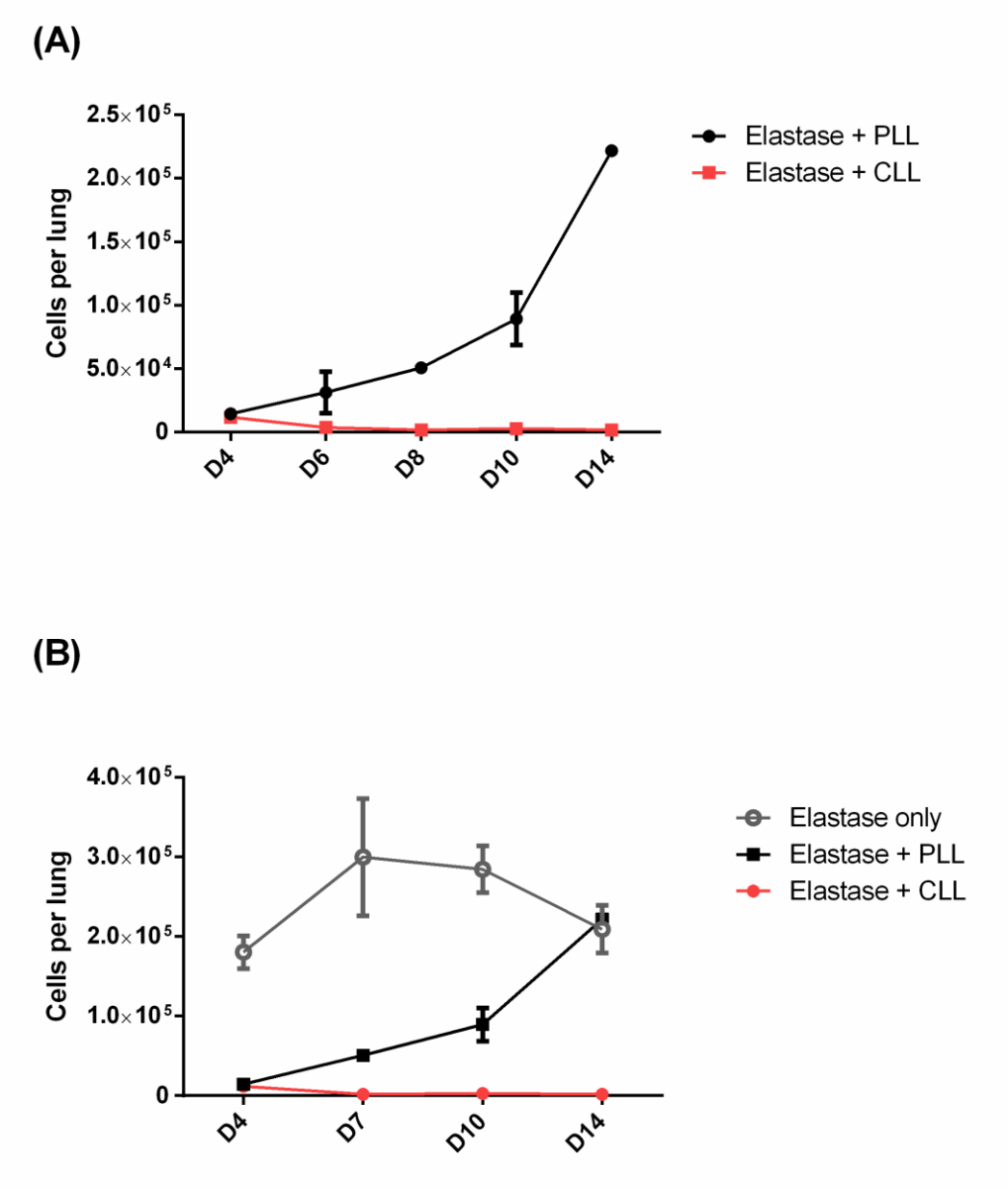


**FIGURE 16 Resident alveolar macrophage dynamics in the lung following elastase administration** (A) Dynamics of resident alveolar macrophage ($CD64^+$, $CD11c^+$, $SiglecF^+$, $CD11b^+$, $PKH26\text{-}PCL^+$) following administration of E+PLL or E+CLL, n=3/group (B) Dynamics of resident alveolar macrophages in mice who received elastase and liposomes or elastase-only (data from Aim 1).

*Interstitial macrophages*

Interstitial macrophages are generally considered to be unaffected by IT and IV administration of CLL – possibly due to their microanatomical location or an inherent decreased phagocytic capacity[107,108]. Indeed, in comparing the number of interstitial macrophages in mice who received E+CLL with those who either received E+PLL or elastase-only, the E+CLL mice actually had a proliferation of cells rather than a depletion.

**Figure 17A** shows the overall dynamics of interstitial macrophages in E+PLL vs E+CLL mice. The interstitial macrophages double between the first and second dose of CLL while there is a gradual decline in the number of resident interstitial macrophages from the first dose of PLL to 7 days after the third dose. Between 24 and 72 hours after the third dose of CLL there is another, albeit smaller, proliferation of the resident population, which then declines to a similar sized population seen in elastase-only mice by day 14 (**Figure 17B**).

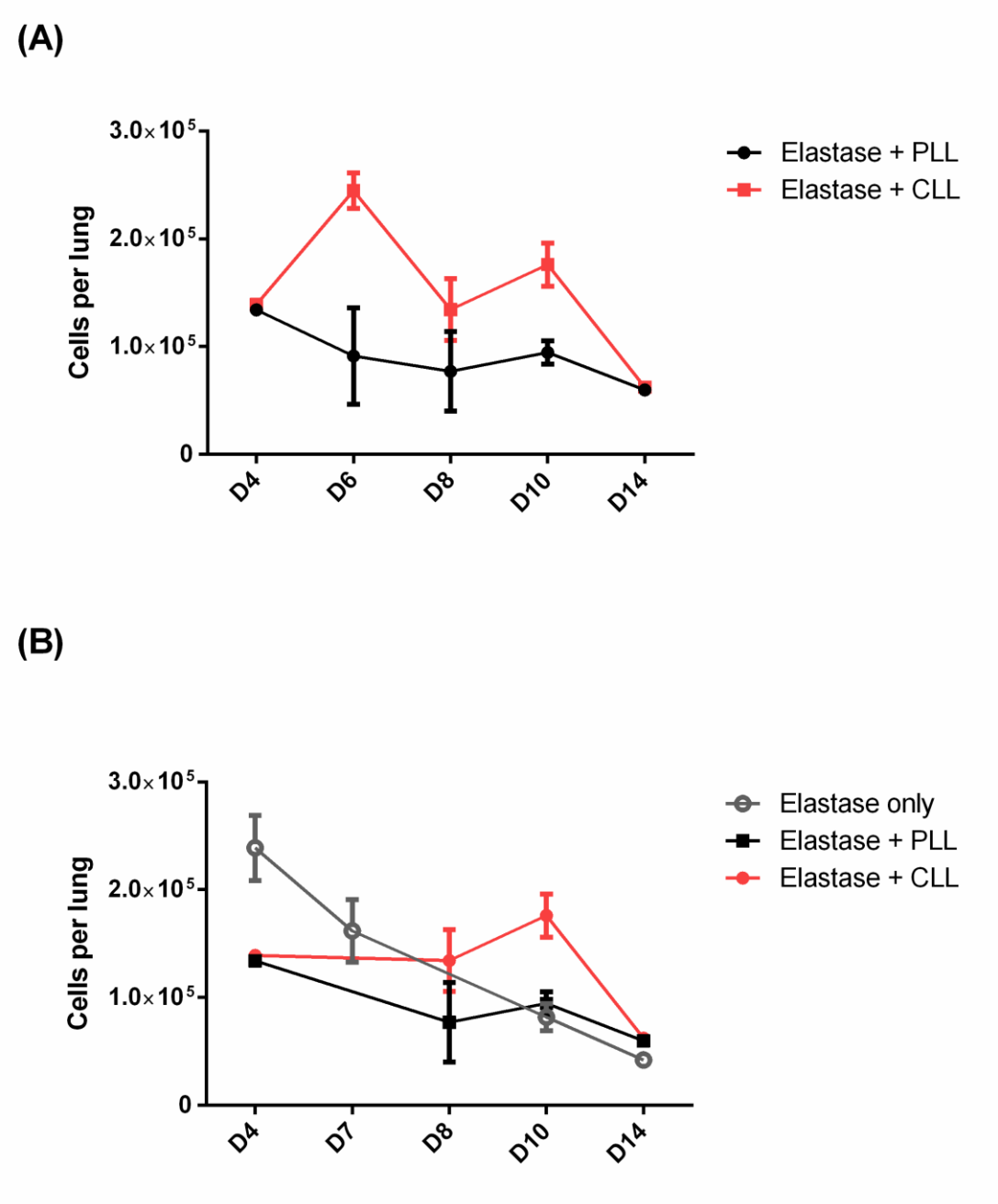


**FIGURE 17 Interstitial macrophage dynamics in the lung following elastase and liposome treatment** (A) Interstitial macrophage dynamics of mice who received elastase (D0) and PLL or CLL, n=3/group (B) Interstitial macrophage dynamics of mice who received elastase and liposomes or elastase-only (data from Aim 1).

*Ly6C+ monocytes*

The Ly6C$^+$ monocyte population decreases between the first and second doses of CLL by about half (**Figure 18A**). This population subsequently peaks between 24 and 72 hours following the third dose of liposomes until declining to baseline 5 days later. The decline in Ly6C$^+$ monocytes between the first and second CLL doses could be due to phagocytosis of liposomes by the first round of infiltrating cells or of Ly6C$^+$ monocytes changing their phenotype and differentiating into interstitial macrophages.

In the PLL treated mice, there is a steady increase in the number of Ly6C$^+$ monocytes throughout the measured time course that culminates in a population of monocytes that is triple the population following the first dose of PLL (**Figure 18B**).

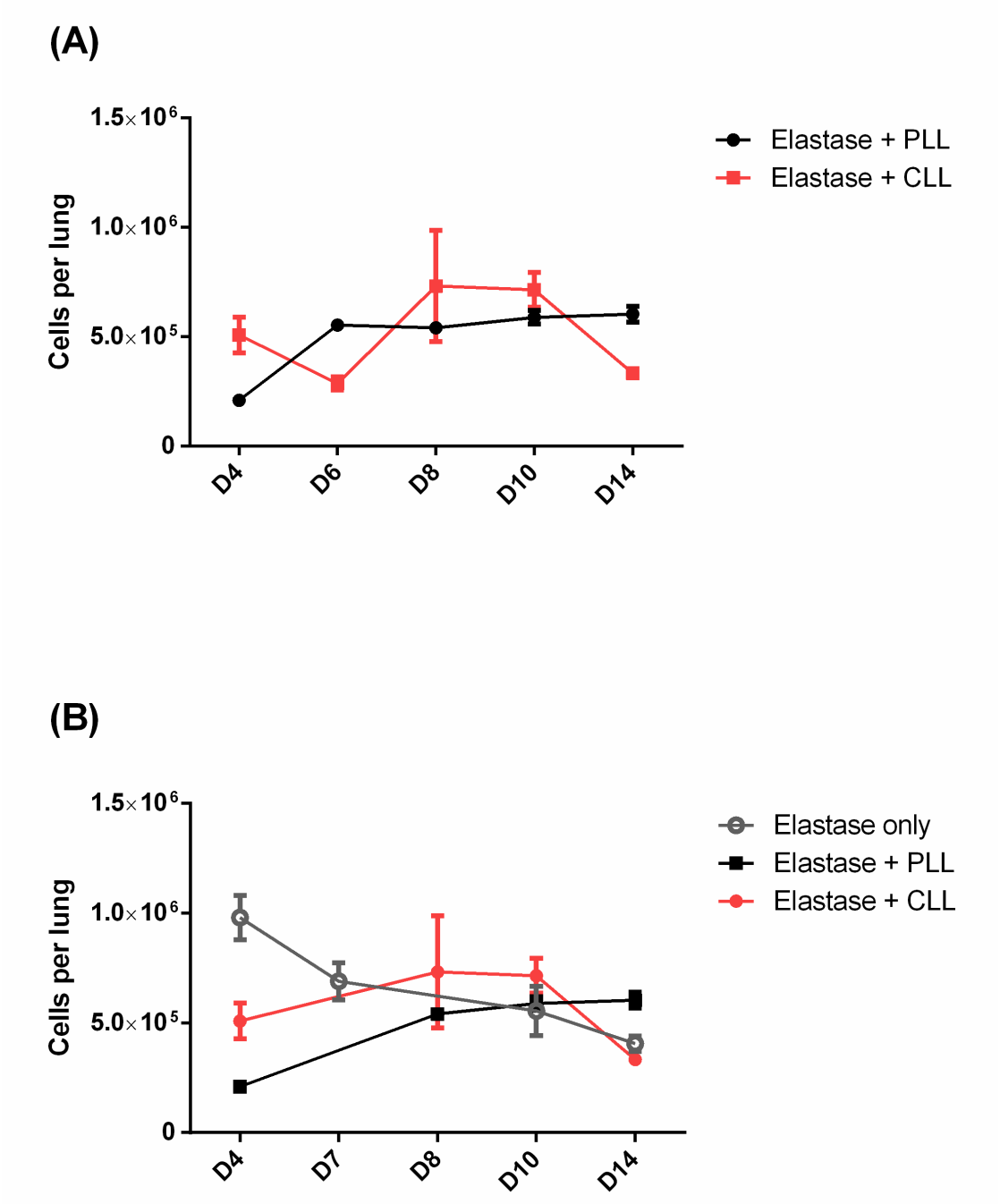


**FIGURE 18 Ly6C⁺ monocyte dynamics in the lung following elastase and liposome treatment** (A) Ly6C⁺ monocyte dynamics in mice who received E+PLL or E+CLL, n=3/group (B) Ly6C⁺ monocyte dynamics in mice who received elastase and liposomes or elastase-only (data from Aim 1).

*Neutrophils*

The neutrophil population following the first dose of CLL is about 3-fold higher than the population following PBS-loaded liposome treatment, likely due to neutrophils being recruited to clean up apoptosed macrophages (**Figure 19A**). This is supported by the emergence of a PKH26-PCL$^{+}$ population of neutrophils following clodronate-loaded liposome administration which occurred at least 8 days following PKH26-PCL administration.

Between the first and second dose of CLL, the neutrophil population in the lung decreases by about 1.6 million cells but rebounds 3-fold that after the third dose of CLL. By day 7 following the third dose of CLL, the neutrophil population is similar to that of mice who received PLL and elastase-alone mice at day 14 post-elastase (**Figure 19B**).

**FIGURE 19**

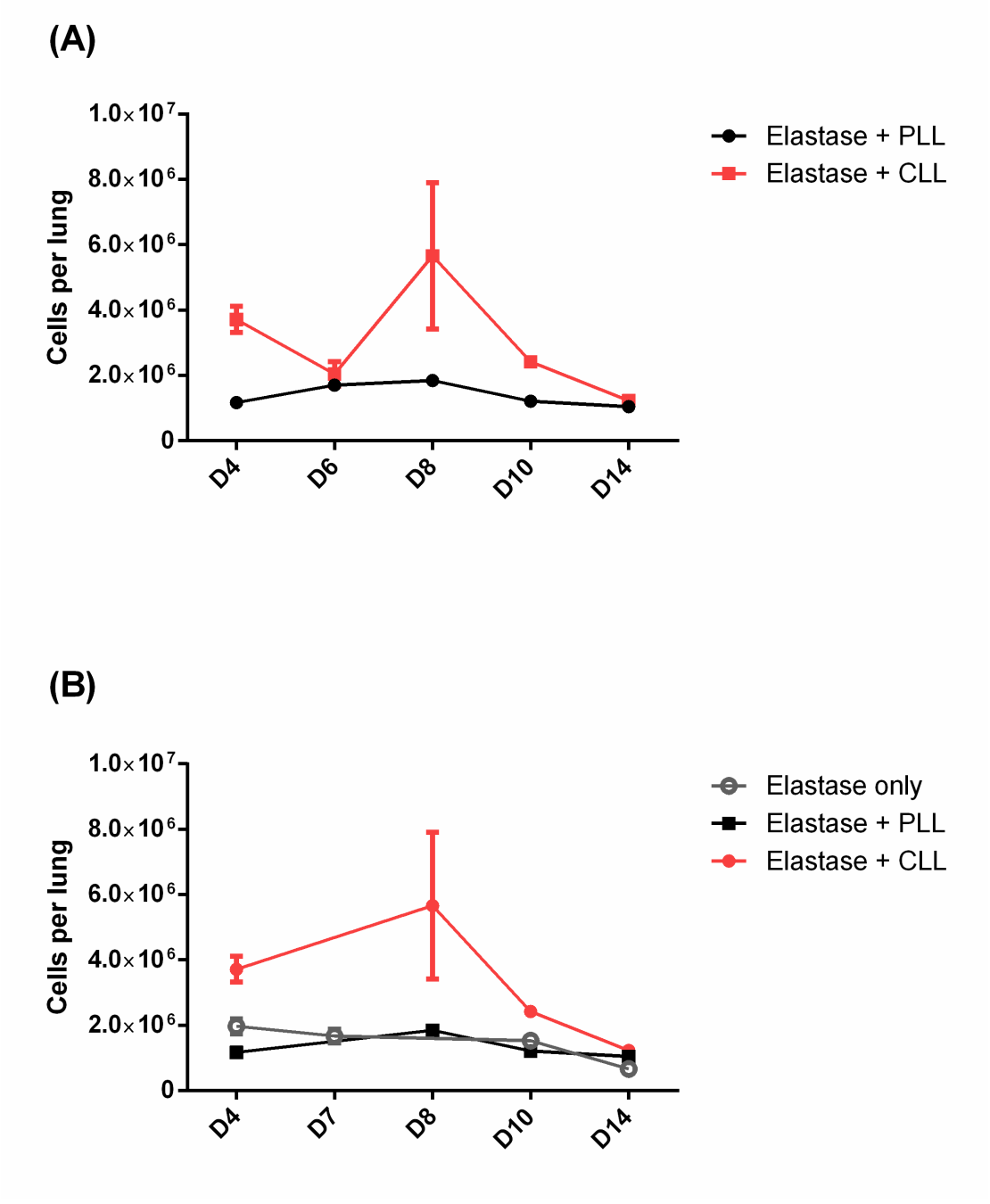


**Neutrophil dynamics in the lung following elastase and liposome treatment** (A) Neutrophil dynamics in mice who received E+PLL or E+CLL, n=3/group (B) Neutrophil dynamics in mice who received elastase and liposomes or elastase-only (data from Aim 1).

*Pulmonary function following macrophage depletion*

The experimental design for the evaluation of emphysema severity following lung macrophage depletion is summarized below in **Figure 20**.

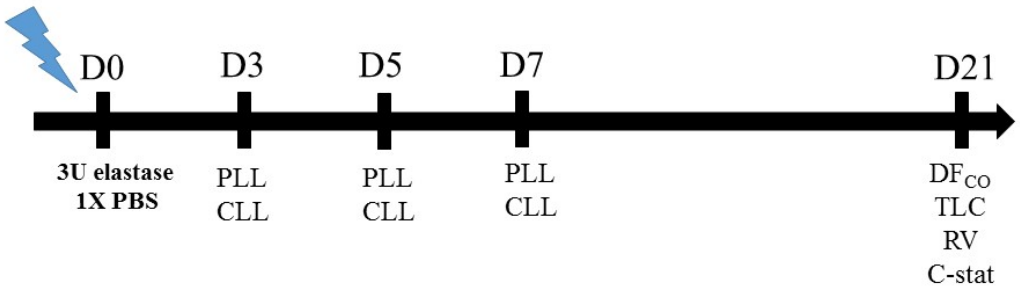


**FIGURE 20 Experimental design for the analysis of the effect of macrophage depletion on emphysema severity** Mice were given either 50 µL of sterile 1X PBS or 3U of elastase in 50 µL of sterile 1X PBS on D0 and received a total of 3 doses of 100µL of CLL or PLL on days 3, 5, and 7 post-elastase. Mice were sacrificed and underwent pulmonary function testing on day 21 post-elastase.

Abbreviations: *$DF_{CO}$*, diffusion factor for carbon monoxide; *TLC,* total lung capacity; *RV,* residual volume; *C-stat*, quasi-static compliance.

*Diffusion factor for carbon monoxide*

The $DF_{CO}$ is a measure of the functional capacity of the alveolar-capillary interface and is analogous to the $DL_{CO}$ used in humans. Values range from 0-1, with 0 being no uptake of carbon monoxide into the blood, and 1 being complete uptake. Low $DF_{CO}$ or $DL_{CO}$ values can be associated with various pathologies including decreased alveolar surface area and capillary blood volume as seen in emphysema[109], cellular infiltration and edema as seen in pulmonary infection, and interstitial thickening as seen in pulmonary fibrosis.

**Figure 21A** summarizes $DF_{CO}$ measurements from mice who received elastase or PBS control and either CLL or PLL liposomes as well as the standard data for healthy (PBS-only) and emphysematous (elastase-only) BALB/cJ mice, as previously determined in the lab. The $DF_{CO}$ values for mice who received E+CLL were significantly lower than mice who received E+PLL (mean ± standard error (SE), 0.5522 ± 0.01325 vs 0.6286 ± 0.01577, p=0.0049) as well as mice

who received elastase-only (0.6965 ± 0.01190, p<0.0001). Notably, there was no significant difference in the $DF_{CO}$ of mice who received E+PLL and mice who received elastase-only, which would suggest that the noted differences are independent of any liposome-mediated processes and are instead through some mechanism related to the depletion of alveolar macrophages. Conversely, in comparing the $DF_{CO}$ of PBS+PLL mice and PBS-only mice, there is a statistically significant difference, however, this may not be physiologically significant (difference between means: -0.03390 ± 0.01363).

*Total lung capacity*

Total lung capacity is a measure of the maximal inflation volume of the lung. TLC in mice is calculated at a pressure of 35 $cmH_2O$. Lung hyperinflation, a hallmark of emphysema, is pathologically associated with increased compliance of the lung and clinically results in increased air trapping and labored breathing[110].

In mice who received E+PLL or E+CLL, the TLC was significantly greater than that of mice who received elastase-only (**Figure 21B)**. The TLC of mice who received E+PLL was 23% greater than elastase-only mice (p=0.0012) and it was 33% greater in mice who received E+CLL compared to elastase-only mice (p<0.0001).

In mice who received PBS+CLL, the TLC was 11% greater than mice who received PBS-only (p=0.0089) and was 9% greater than mice who received PBS+PLL (p=0.0172). There was no significant difference in the TLC of mice who received PBS-only or PBS+PLL.

*Residual volume*

The residual volume (RV) is the amount of air that is trapped in the lung following forced expiration or in the case of laboratory animals, following deflation of the lung. Residual volume is

increased in emphysema where there is decreased elastic recoil, a characteristic of the lung necessary to force inspired air out[33].

The RV in mice treated with E+CLL is 28% greater than in mice treated with elastase-only (p=0.0240) and is 32% greater than in mice treated with E+PLL (p=0.0185) (**Figure 21C**). There is no significant difference in RV between mice treated with E+PLL and mice treated with elastase-only. Further, the administration of PLL or CLL showed no effect on RV in PBS treated mice.

*Quasi-static compliance*

Compliance is a pulmonary function metric that indicates how easily the lung expands at a given pressure and is influenced by the elasticity of lung tissue as well as the surface tension in the alveoli. In patients with emphysema, the compliance of the lung is significantly increased due to the decreased elastic recoil of the lung and increased surface tension in the alveoli related to their decreased surface area.

Mice who received E+ PLL or E+CLL, had a significant increase in lung compliance compared to mice treated with elastase-only (17%, P=0.0057 and 18%, p=0.0070, respectively) (**Figure 21D**). Conversely, mice treated with PBS+CLL and not PBS+PLL, had a significant increase in lung compliance compared to mice treated with PBS-only or PBS+PLL (10%, p=0.0495 and 16%, p=0.0072, respectively).

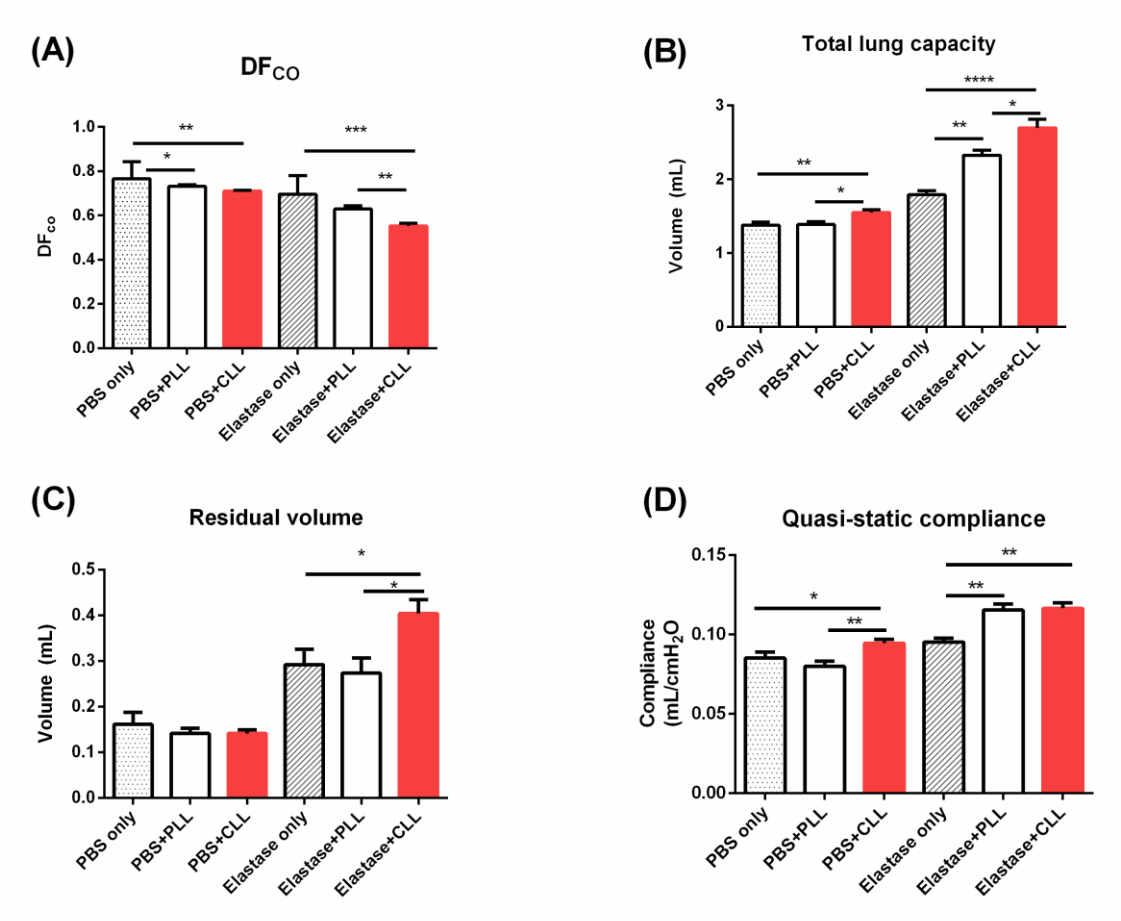


**FIGURE 21 Pulmonary function tests following elastase and liposome treatment** Data for PBS-only and elastase-only groups are from previous pooled experiments in our lab where PBS-only indicates male BALB/cJ mice given 50 µL 1X PBS IT on D0 and elastase-only indicates male BALB/cJ mice given 3 U elastase suspended in 50 µL 1X PBS IT on D0 with all pulmonary function measures performed on day 21 post-elastase. PBS+PLL/CLL = 1X PBS IT on D0, PLLCLL on D3, D5, D7; Elastase+PLL/CLL= 3 U elastase IT on D0, PLLCLL on D3, D5, D7; with all pulmonary function measures performed on day 21 post-elastase. n=5 for all groups except n=6 for E+PLL. *t*-test analysis between groups as indicated by the horizontal line. * = $p < 0.05$, ** = $p < 0.01$, *** = $p < 0.001$

# DISCUSSION

## Flow cytometry

To gain a more complete understanding of the cellular environment following elastase challenge in BALB/cJ mice, flow cytometry was employed. While previous research in the lab had characterized cells in the BAL, this methodology is susceptible to inefficient and variable recovery of cells, the possibility that elastase challenge enhances recovery of cells, and limited ability to sample cells from the interstitial or vascular compartments. The lab has also performed preliminary characterization of myeloid cells using flow cytometry on whole lung homogenates, however, this was performed using a BD FACSCalibur which is limited to four fluorescent parameters and given the sensitivity of the FITC channel to auto-fluorescence, our research was primarily limited to three fluorescent parameters. This methodology, while useful for preliminary analysis, did not allow us to capture a detailed snapshot of cellular dynamics. Further, due to the limitation of the number of fluorochromes that could be used on the FACSCalibur, we were unable to gate out dead cells which can impact flow cytometry interpretation as antibodies can non-specifically bind to dead cells.

A 10-color flow cytometry panel was developed based on current literature and previous work in the lab[19,111,112]. Antibodies were optimized to minimize the influence of auto-fluorescence and provide the best discrimination between cellular populations. To distinguish $CD11b^+$ dendritic cells (DCs) from interstitial macrophages, we used the high-affinity Fc-γ receptor I (FcγRI), CD64, which is only expressed on macrophages, monocytes, and some neutrophils[113]. Of note, we did not focus on dendritic cell populations in this analysis but with the inclusion of additional markers such as CD103 and CD24 this could be accomplished.

Our decision to identify only $Ly6C^+$ monocytes was the product of poor availability of antibodies that could clearly discriminate infiltrating monocyte subpopulations. Characteristically, there are thought to be two main monocyte populations: “classical” monocytes, which emigrate

from the bone marrow and infiltrate sites of inflammation, and "patrolling" monocytes, which circulate throughout the body during steady-state conditions and replenish certain macrophage and dendritic cell populations. Classical monocytes are typically characterized by their high expression of Ly6C and the chemokine receptor CCR2, as well as adhesion molecules including, but not limited to, L-lectin (CD62L), P-selectin glycoprotein ligand 1 (PSGL1), lymphocyte function-associated antigen 1 (LFA1), and macrophage receptor 1 (MAC1)[95,114,115]. While in circulation, $Ly6C^+$ monocytes transition into $Ly6C^-$ monocytes. Patrolling monocytes are defined by a low expression of Ly6C and a high expression of the chemokine receptor $CX_3CR1$.

If a suitable antibody panel can be derived, future investigation into the contribution of $Ly6C^-$ monocytes to the lung macrophage populations and their role in disease severity and progression should occur as they appear to play significant and disparate roles in other sterile inflammation models. For instance, using a liver fibrosis murine model, Ramachandran and colleagues demonstrated that $Ly6C^-$ monocytes were the main source of MMPs during liver wound healing and scar remodeling whereas $Ly6C^+$ monocytes were primarily responsible for the formation of fibrotic tissue[116]. Conversely, during healing following myocardial infarction, $Ly6C^+$ monocytes have been associated with proteolytic, inflammatory functions and $Ly6C^-$ monocytes have been associated with the orchestration of accumulation of myofibroblasts, collagen deposition, and angiogenesis[117]. Continuing to develop antibodies with improve specificity and sensitivity will undoubtedly aid in our understanding of the complex immune environment in the lung following elastase challenge.

**Aim 1:** ***Elucidate the dynamics of resident and recruited macrophages, monocytes, and neutrophils in the lung following administration of elastase in BALB/cJ mice.***

In order to test the effect of macrophage depletion on the severity and progression of elastase-induced emphysema, it was necessary to first evaluate the cellular dynamics following administration of elastase in BALB/cJ mice. We found that the alveolar macrophage population

(CD64$^{+}$, CD11c$^{+}$, SiglecF$^{+}$) underwent an initial contraction with 2.6-fold fewer cells at day 4 post-elastase compared to the naïve lung which then rebounded to about 3/4 that of the naïve lung at day 10 and subsequently declined to about half the population of the naïve lung by day 14. We hypothesize that this contraction is due either to macrophage cell death (apoptosis, autophagy, or oncosis) secondary to efferocytosis of infiltrating neutrophils or macrophage migration to the draining lymph node following neutrophil efferocytosis. Under normal inflammatory conditions, macrophages engulf apoptopic leukocytes to avoid their secondary necrosis and aid in the resolution of inflammation. During this process, they accumulate reactive oxygen species which are normally controlled and migrate to the draining lymph nodes. However, in many chronic inflammatory conditions such as artherosclerosis, macrophages undergo excessive oxidative burst secondary to the phagocytosis of apoptotic cells and become apoptotic themselves[118,119]. In order to further delineate the alveolar macrophage dynamics in our model, studies evaluating the draining lymph nodes by flow cytometry and in vitro microscopy assays to evaluate cell death should be performed.

To evaluate if the increase in the number of alveolar macrophages at day 7 was due to local proliferation of the resident population or differentiation of recruited peripheral blood monocytes, we employed PKH26-PCL staining to selectively label the phagocytic cells in the lung prior to elastase administration (defined broadly as resident lung macrophages). Our results indicate that vast majority of expansion on day 7 can be attributed to local proliferation of the resident population. The proliferation that occurred between days 4 and 7 could be due to a number of growth signals following macrophage efferocytosis of neutrophils, the influx of lymphocytes, or cytokine expression from ILC2s around this time point. A study evaluating resolution of inflammation in bacterial pneumonia found that alveolar macrophages produced hepatocyte growth factor (HGF) upon phagocytosis of inflammatory neutrophils and similarly saw an increase in the number of alveolar macrophages between ~2-5 days post-infection followed by a decline until day 14 post-infection[120]. While they did not evaluate macrophage HGF receptor

expression, it is possible that HGF is exerting an autocrine effect as macrophages. In the peritoneum and brain, macrophages have been demonstrated to express the receptor, c-met, and undergo proliferation in response to HGF[121]. Given the temporal nature of the proliferation, it is feasible that infiltrating T cells could be producing GM-CSF or some other factor that leads to macrophage proliferation.

Notably, there is a steadily increasing population of PKH26-PCL$^-$ alveolar macrophages that could either be from recruited or unlabeled resident cells, however, the dynamics of this population do not mirror those of the PKH26-PCL$^+$ population, thus it's plausible that these are recruited cells. While alveolar macrophages are traditionally defined as being CD11b$^-$ in steady state, during the acute inflammatory phase, a subpopulation of alveolar macrophages upregulates expression of CD11b. This population peaks by day 7 at a 5-fold increase over the naïve lung, and subsequently returns to baseline by day 14. Stratification by PKH26-PCL indicates that the majority of these cells are from the resident population, but there does exist a much smaller population of PKH26-PCL$^-$ population with a similar dynamic as the CD64$^+$, CD11c$^+$, SiglecF$^+$, PKH26-PCL$^-$ alveolar macrophage population.

Though all of the alveolar macrophage populations evaluated returned to near baseline levels, the interstitial macrophage population remained slightly elevated by day 14 after undergoing expansion following the administration of elastase through day 4 and subsequently declining. Because we only collected data through day 14, it's unclear if this population remains slightly elevated or if it continues to contract. Because interstitial macrophages are seeded from peripheral blood monocytes and can replenish alveolar macrophages in cases of depletion, we were interested in seeing whether they underwent local proliferation or were of monocyte origin. Unfortunately, the labeling of interstitial macrophages was not effective thus this data cannot be interpreted with confidence. Interestingly, the PKH26-PCL positive and negative populations appear to expand and contract in parallel, thus it's plausible that they are of the same population.

In order to further elucidate the dynamics of interstitial macrophages and PKH26-PCL$^-$ alveolar macrophages, it is necessary to do a similar experiment where peripheral leukocytes are labeled. For instance, bone marrow chimeras where donor hematopoietic cells express green fluorescent protein (GFP) and the host resident lung cells are conserved during irradiation by a lung shield would allow for tracking of recruited cells into the lung as was performed by Janssen et al. 2011[25]. Unfortunately, there are currently no commercially available BALB/cJ transgenic mice that we could use for this and while there is a commercially available BALB/cByJ (MHC haplotype matched with BALB/cJ) GFP mouse (CByJ.B6-Tg(UBC-GFP)30Scha/J, Stock No. 007076, The Jackson Laboratory, Bar Harbor, ME) the strain-dependent phenotypic differences we've noted in the elastase model likely preclude this as a viable option to study recruited leukocytes.

Finally, as part of defining the immune cell dynamics following elastase, we looked at neutrophils and Ly6C$^+$ monocytes. The dynamics of both populations were as expected with an early infiltration peaking on day 2 for neutrophils and day 4 for monocytes. As mentioned previously, future experiments should aim to delineate the dynamics and gene expression profiles of the two monocyte populations for their role in emphysema.

**Aim 2:** ***Determine if the depletion of resident lung macrophages ameliorates or worsens elastase-induced emphysematous changes in the lungs of BALB/cJ mice.***

Based on these data, we decided to deplete lung macrophages between days 3 and 7 following elastase administration as this was the period leading up to the day 7 expansion and phenotypic change in the alveolar macrophage population to a mixed M1/M2 phenotype (previous data from the lab, not shown). We found that administering a total of three doses of CLL IT on days 3, 5, and 7 post-elastase was 85-98% efficacious at depleting alveolar macrophages with the highest degree of depletion occurring 24 hours after the third dose. Notably, the depletion was maintain at around 92% one week following the third dose of CLL. Interestingly, the administration of PLL appeared to cause a degree of alveolar macrophage depletion as E+PLL mice

had almost an order of magnitude fewer alveolar macrophages than elastase-only mice. We similarly noted that the dynamics of interstitial macrophages, Ly6C$^+$ monocytes, and neutrophils in CLL and PLL treated mice were disparate from the elastase-only mice. This finding is not surprising as 1) we are giving a repeated dose of 100 μL of liquid into the lungs which at the very least will cause some level of inflammation and likely also introduce bacteria from the upper airways into the delicate peripheral airways and 2) the mass depletion of macrophages will induce an inflammatory response in itself, confounding our study of the immune environment on emphysema severity and progression. For these reasons, the whole lung depletion of macrophages is not the ideal technique to study the contribution of macrophages to emphysema.

In order to evaluate the effect of macrophage depletion on emphysema severity, we performed pulmonary function tests to obtain measurements of $DF_{CO}$, TLC, RV, and quasi-static compliance. We found that the $DF_{CO}$ for elastase-treated mice with depleted macrophages was significantly lower than mice with intact macrophages, indicating decreased gas-exchange capacity of the parenchymal lung tissue. This effect appeared to be independent of liposome administration as there was no difference in elastase-only and E+PLL mice. The TLC between elastase-treated mice receiving CLL was significantly greater than both E+PLL and elastase-only treated mice. Additionally, the TLC of E+PLL mice was greater than that of elastase-only mice. Similar results were noted with the quasi-static compliance, however, there was no significant difference between E+CLL and E+PLL mice. These data are difficult to interpret because in the PBS control-treated mice, a liposome-dependent effect was not noted but a macrophage depletion effect was. Perhaps, in the injured elastase-treated lung, the administration of PLL exacerbates the inflammatory milieu in the lung leading to increased tissue destruction and thus greater TLC and compliance. Additionally, while we did not track the cellular dynamics of PBS+PLL or PBS+CLL mice needed to evaluate this finding, in the E+PLL mice, there was a notable decrease in the number of alveolar macrophages compared to elastase-only animals. It's possible that the administration of PLL exacerbated the natural early decline in alveolar macrophages in this

elastase model system either through liposome phagocytosis-induced macrophage apoptosis or migration to the draining lymph nodes.

In both TLC and quasi-static compliance measurements, there's a significant difference between PBS-treated mice with depleted macrophages and PBS-only or PBS+PLL mice, indicating that the depletion of macrophages alone can cause parenchymal destruction. This leads to increased compliance and decreased elastance of the lung. Interestingly, this effect is not noted in the measure of residual volume as one would expect, however, this is the least sensitive of the three measures. The residual volume was significantly increased in elastase-treated mice with depleted macrophages compared to E+PLL and elastase-only mice and there was no change in residual volume noted in our control mice. Taken together, the pulmonary function results suggest that in both naïve (PBS-treated) and emphysematous (elastase-treated) lungs, the depletion of macrophages results in decreased gas exchange capacity of the lung parenchyma, increased compliance, decreased elastic recoil, and subsequently increased total lung capacity. These effects are exacerbated in the emphysematous lung.

# CONCLUSION

The hypothesis of this study, that depletion of macrophages prior to their transition to an M2/M1 phenotype around day 7 would ameliorate emphysema severity, was not supported by the data. The simplistic interpretation of the results is that depletion of macrophages worsens the severity of emphysema. However, the control arms of the depletion experiments strongly indicate that there are serious technical issues with liposome administration in the lungs that have a profound influence on the final phenotype.

At one level, it is not particularly surprising that macrophage depletion resulted in enhanced pathology. Macrophages are instrumental in wound repair and the limiting of inflammation in the lung, as discussed in the introduction. To deplete macrophages entirely would abrogate not only the dysregulated, destructive repair mechanisms we hypothesize to be occurring in our emphysema model but any protective, reparative mechanism they are capable of exerting as well. Additionally, the repeated administration of a viscous liquid into the lungs and the macrophage depletion events themselves appear to exert an immune modulating effect that confounds interpretation of our results. To illustrate the disparate roles that macrophages can play in chronic lung disease, one can compare emphysema with idiopathic pulmonary fibrosis (IPF). Both disease pathogeneses show a strong association with lung macrophages, however in

IPF there's excessive extracellular matrix deposition and not enough tissue remodeling[122] whereas in emphysema, there seems to be a lack of matrix deposition with excessive remodeling[89].

The data from this study indicate that macrophages do play an important role in emphysema progression and severity however, the methodology to evaluate their mechanisms of action would be better approached from a reprogramming angle rather than full depletion[123]. Previous research in the lab has indicated that an immune environment in the lungs that favors Th1/M1 skewing, as seen in the more resistant C57Bl/6J mouse and in mice with decreased severity of emphysema following viral infection, may be protective[57]. To this end, macrophage-targeted therapy might be a promising option not only to study the mechanisms of action of macrophage but as a therapy to halt emphysema progression in human patients.

The macrophage phenotype can be altered in a number of ways including, but not limited to, the *in situ* administration of IRF/STAT signaling pathway agonists and inhibitors, growth factors, and the adoptive transfer of macrophages phenotypically skewed *in vitro*[124]. The effects of adoptively transferring macrophages polarized *in vitro* or through genetic manipulation of a known defective gene to rodent models of disease has recently proven successful in rescuing spinal cord injury in rats[125], endotoxemia in mice[126], and hereditary pulmonary alveolar proteinosis (herPAP) in mice[127]. Importantly, macrophage therapy appears to have the capacity for a long lasting effect as demonstrated in the transplantation of macrophage progenitors to treat a murine model of the hereditary form of pulmonary alveolar proteinosis (PAP), a lung disease caused by mutations in the gene encoding GM-CSF. With a single treatment of macrophage progenitors, the cells engrafted and differentiated into functional macrophages capable of significantly ameliorating PAP symptoms for at least 9 months[128]. Additionally, the direct administration of polarizing stimuli including interferon (IFN)-γ[129] (towards M1) and IL-4[130] (towards M2) has demonstrated improved resolution of infection and inflammation, respectively. Notably, this blanket administration of stimuli that act on a variety of cells could have negative off-

target effects, thus a focused intervention specific to macrophages would be ideal. Indeed, the use of a chemically modified viral nanoparticles to deliver polarizing agents to macrophages *in vitro* was recently demonstrated not only to specifically target macrophages but to be sequestered differentially by M1/M2 phenotype[131].

Emphysema is a complex immunological disease that involves multiple cell types, effector molecules, genes, and environmental factors. The work in this thesis gives a glimpse into the complexities of myeloid cell dynamics following the onset of elastase-induced lung damage and contributes to our appreciation for the role of the lung macrophage in the progressive alveolar destruction seen in our model. Future studies incorporating monocyte tracking, macrophage reprogramming, and gene expression analysis will help further delineate the dynamics and role of macrophages in emphysema.

# REFERENCES


1. Vestbo J, Hurd SS, Agustí AG, et al. Global strategy for the diagnosis, management, and prevention of chronic obstructive pulmonary disease GOLD executive summary. *Am J Respir Crit Care Med*. 2013;187(4):347-365. doi:10.1164/rccm.201204-0596PP.

2. WHO. The top 10 causes of death. 2014. http://www.who.int/mediacentre/factsheets/fs310/en/. Accessed March 8, 2016.

3. López-Campos JL, Tan W, Soriano JB. Global burden of COPD. *Respirology*. 2015;(October 2015):n/a - n/a. doi:10.1111/resp.12660.

4. Barnes PJ. Why More Research into Molecular and Cellular Mechanisms of COPD Is Needed. In: Barnes PJ, ed. *Chronic Obstructive Pulmonary Disease Cellular and Molecular Mechanisms*. Vol Boca Raton, FL: Taylor & Francis Group; 2005:1-16.

5. Suarez CJ, Dintzis SM, Frevert W. Respiratory. In: Treuting PM, Dintzis SM, eds. *Comparative Anatomy and Histology: A Mouse and Human Atlas*. Vol San Diego: Academic Press; 2011:121-134.

6. Levitzky MG. Chapter 1: Function & Structure of the Respiratory System. In: *Pulmonary Physiology*. Vol 6th ed. New York: McGraw-Hill; 2003:1-10.

7. Weibel ER. Chapter 10: Airways and Blood Vessels. In: *The Pathway for Oxygen*. Vol 1st ed. Cambridge: Harvard University Press; 1984:272-301.

8. Weibel ER. It takes more than cells to make a good lung. *Am J Respir Crit Care Med*. 2013;187(4):342-346. doi:10.1164/rccm.201212-2260OE.

9. Weibel ER. What makes a good lung? *Swiss Med Wkly Off J Swiss Soc Infect Dis Swiss Soc Intern Med Swiss Soc Pneumol*. 2009;139(27-28):375-386. doi:smw-12270.

10. Ochs M, Nyengaard JR, Jung A, et al. The number of alveoli in the human lung. *Am J Respir Crit Care*

*Med*. 2004;169(1):120-124. doi:10.1164/rccm.200308-1107OC.

11. Weibel ER, Gomez M. Architecture of the human lung. *Science*. 1962;137(3530):577-585.

12. Wiebe BM, Laursen H. Human lung volume, alveolar surface area, and capillary length. *Microsc Res Tech*. 1995;32(3):255-262. doi:10.1002/jemt.1070320308.

13. Hasleton PS. The internal surface area of the adult human lung. *J Anat*. 1972;112(Pt 3):391-400.

14. Weibel ER. On the tricks alveolar epithelial cells play to make a good lung. *Am J Respir Crit Care Med*. 2015;191(5):504-513. doi:10.1164/rccm.201409-1663OE.

15. Mason RJ. Biology of alveolar type II cells. *Respirology*. 2006;11 Suppl:S12-S15. doi:10.1111/j.1440-1843.2006.00800.x.

16. Barkauskas CE, Cronce MJ, Rackley CR, Bowie EJ, Keene DR, Stripp BR, Randell SH, Noble PW HB. Type 2 alveolar cells are stem cells in adult lung. *J Clin Invest*. 2013;123(7):3025-3036. doi:10.1172/JCI68782DS1.

17. Sannes PL, Wang J. Basement membranes and pulmonary development. *Exp Lung Res*. 1997;23(2):101-108. doi:10.3109/01902149709074023.

18. Balestrini JL, Niklason LE. Extracellular Matrix as a Driver for Lung Regeneration. *Ann Biomed Eng*. 2015;43(3):568-576. doi:10.1007/s10439-014-1167-5.

19. Hussell T, Bell TJ. Alveolar macrophages: plasticity in a tissue-specific context. *Nat Rev Immunol*. 2014;14(2):81-93. doi:10.1038/nri3600.

20. Kopf M, Schneider C, Nobs SP. The development and function of lung-resident macrophages and dendritic cells. *Nat Immunol*. 2014;16(1). doi:10.1038/ni.3052.

21. Yona S, Kim KW, Wolf Y, et al. Fate Mapping Reveals Origins and Dynamics of Monocytes and Tissue Macrophages under Homeostasis. *Immunity*. 2013;38(1):79-91. doi:10.1016/j.immuni.2012.12.001.

22. Schulz C, Perdiguero EG, Chorro L, et al. A Lineage of Myeloid Cells independent of Myb and Hematopoietic Stem Cells. *Science (80- )*. 2012;336(April):86-90. doi:10.1126/science.1219179.

23. Takahashi K, Yamamura F, Naito M. Differentiation, maturation, and proliferation of macrophages in the mouse yolk sac: a light-microscopic, enzyme-cytochemical, immunohistochemical, and ultrastructural study. *J Leukoc Biol*. 1989;45(2):87-96.

24. Guilliams M, De Kleer I, Henri S, et al. Alveolar macrophages develop from fetal monocytes that differentiate into long-lived cells in the first week of life via GM-CSF. *J Exp Med*. 2013;210(10):1977-1992. doi:10.1084/jem.20131199.

25. Janssen WJ, Barthel L, Muldrow A, et al. Fas determines differential fates of resident and recruited macrophages during resolution of acute lung injury. *Am J Respir Crit Care Med*. 2011;184(5):547-560. doi:10.1164/rccm.201011-1891OC.

26. Morales-Nebreda L, Misharin A V., Perlman H, Scott Budinger GR. The heterogeneity of lung macrophages in the susceptibility to disease. *Eur Respir Rev*. 2015;24(137):505-509. doi:10.1183/16000617.0031-2015.

27. Cai Y, Sugimoto C, Arainga M, Alvarez X, Didier ES, Kuroda MJ. In vivo characterization of alveolar and interstitial lung macrophages in rhesus macaques: implications for understanding lung disease in humans. *J Immunol*. 2014;192(6):2821-2829. doi:10.4049/jimmunol.1302269.

28. Maus UA, Janzen S, Wall G, et al. Resident alveolar macrophages are replaced by recruited monocytes in response to endotoxin-induced lung inflammation. *Am J Respir Cell Mol Biol*. 2006;35(2):227-235. doi:10.1165/rcmb.2005-0241OC.

29. Matute-Bello G, Lee JS, Frevert CW, et al. Optimal timing to repopulation of resident alveolar macrophages with donor cells following total body irradiation and bone marrow transplantation in mice. *J Immunol Methods*. 2004;292(1-2):25-34. doi:10.1016/j.jim.2004.05.010.

30. Landsman L, Jung S. Lung Macrophages Serve as Obligatory Intermediate between Blood

Monocytes and Alveolar Macrophages. *J Immunol*. 2007;179(6):3488-3494. doi:10.4049/jimmunol.179.6.3488.

31. Snelgrove RJ, Goulding J, Didierlaurent AM, et al. A critical function for CD200 in lung immune homeostasis and the severity of influenza infection. *Nat Immunol*. 2008;9(9):1074-1083. doi:10.1038/ni.1637.

32. GOLD. Spirometry for Health Care Providers. *Glob Iniative Chronic Obstr Pulm Dis*. 2010:1-14. http://www.goldcopd.org/uploads/users/files/GOLD_Spirometry_2010.pdf. Accessed January 15, 2016.

33. Macklem P. Reexamination of the elastic properties of emphysematous lungs. *Respiration*. 1990;57(3):187-192.

34. Eisner MD, Anthonisen N, Coultas D, et al. An Official American Thoracic Society Public Policy Statement: Novel Risk Factors and the Global Burden of Chronic Obstructive Pulmonary Disease. *Am J Respir Crit Care Med*. 2010;182(5):693-718. doi:10.1164/rccm.200811-1757ST.

35. Svanes C, Sunyer J, Plana E, et al. Early life origins of chronic obstructive pulmonary disease. *Thorax*. 2010;65(1):14-20. doi:10.1136/thx.2008.112136.

36. Salvi SS, Barnes PJ. Chronic obstructive pulmonary disease in non-smokers. *Lancet*. 2009;374(9706):1964-1965; author reply 1965-1966. doi:10.1016/S0140-6736(09)62116-4.

37. Postma DS, Bush A, van den Berge M. Risk factors and early origins of chronic obstructive pulmonary disease. *Lancet*. 2015;385(9971):899-909. doi:10.1016/S0140-6736(14)60446-3.

38. Blanco I, de Serres FJ, Fernandez-Bustillo E, Lara B, Miravitlles M. Estimated numbers and prevalence of PI*S and PI*Z alleles of alpha1-antitrypsin deficiency in European countries. *Eur Respir J Off J Eur Soc Clin Respir Physiol*. 2006;27(1):77-84. doi:10.1183/09031936.06.00062305.

39. Cox DW, Woo SL, Mansfield T. DNA restriction fragments associated with a1-antitrypsin indicate a

single origin for deficiency allele PI Z. *Nature*. 1985;314:435-438.

40. Laurell C-B, Eriksson S. The Electrophoretic α; 1 -Globulin Pattern of Serum in α; 1 -Antitrypsin Deficiency. *Scand J Clin Lab Investig*. 1963;15(2):132-140. doi:10.1080/00365516309051324.

41. Fletcher C, Peto R. The natural history of chronic airflow obstruction. *Br Med J*. 1977;1(June):1645-1648. doi:10.1136/bmj.1.6077.1645.

42. DeMeo DL, Silverman EK. Alpha1-antitrypsin deficiency. 2: genetic aspects of alpha(1)-antitrypsin deficiency: phenotypes and genetic modifiers of emphysema risk. *Thorax*. 2004;59:259-264. doi:10.1136/thx.2003.006502.

43. CDC. Increase Expected in Medical Care Costs for COPD. 2014. http://www.cdc.gov/features/ds-copd-costs/. Accessed March 8, 2016.

44. Mahadeva R, Shapiro SD. Chronic obstructive pulmonary disease. 3: Experimental animal models of pulmonary emphysema. *Thorax*. 2002;57(10):908-914. doi:10.1136/thorax.57.10.908.

45. Marcelino MY, Fuoco NL, de Faria CA, Kozma RDLH, Marques LF, Ribeiro-Paes JT. Animal models in chronic obstructive pulmonary disease-an overview. *Exp Lung Res*. 2014;40(6):259-271. doi:10.3109/01902148.2014.908250.

46. Martorana PA. The pallid mouse. A model of genetic alpha 1-antitrypsin deficiency. *Lab Investig*. 1993;68(2):233-241.

47. Shibata Y, Zsengeller Z, Otake K, Palaniyar N, Trapnell BC. Alveolar macrophage deficiency in osteopetrotic mice deficient in macrophage colony-stimulating factor is spontaneously corrected with age and associated with matrix metalloproteinase expression and emphysema. *Blood*. 2001;98(9):2845-2852. doi:10.1182/blood.V98.9.2845.

48. Szapiel S V, Fulmer JD, Hunninghake GW, et al. Hereditary emphysema in the tight-skin (Tsk/+) mouse. *Am Rev Respir Dis*. 1981;123(6):680-685.

http://www.ncbi.nlm.nih.gov/entrez/query.fcgi?cmd=Retrieve&db=PubMed&dopt=Citation&list_uids=7271067.

49. Fisk DE, Kuhn C. Emphysema-like changes in the lungs of the blotchy mouse. 1976;113(6):787-797. http://www.ncbi.nlm.nih.gov/entrez/query.fcgi?cmd=Retrieve&db=PubMed&dopt=Citation&list_uids=937819.

50. Yoshida M, Korfhagen TR, Jeffrey A. Surfactant Protein D Regulates NF- κ B and Matrix Metalloproteinase Production in Alveolar Macrophages via Oxidant-Sensitive Pathways. 2014. doi:10.4049/jimmunol.166.12.7514.

51. Hautamaki RD, Kobayashi DK, Senior RM, Shapiro SD. Requirement for Macrophage Elastase for Cigarette Smoke-Induced Emphysema in Mice Author ( s ): R . Dean Hautamaki , Dale K . Kobayashi , Robert M . Senior and Steven D . Shapiro Published by : American Association for the Advancement of Science Stable UR. 2016;277(5334):2002-2004.

52. Morris DG, Huang X, Kaminski N, Wang Y. Loss of integrin a v b 6-mediated TGF- b activation causes Mmp12-dependent emphysema. 2003;12450(1996):169-173.

53. Wright JL, Churg A. Cigarette Smoke Causes Physiologic and Morphologic Changes of Emphysema in the Guinea Pig. 1990;142(6):1422-1428.

54. Churg A, Sin DD, Wright JL. Everything prevents emphysema: Are animal models of cigarette smoke-induced chronic obstructive pulmonary disease any use? *Am J Respir Cell Mol Biol*. 2011;45(6):1111-1115. doi:10.1165/rcmb.2011-0087PS.

55. Gross P, Pfitzer E, Tolker E, Babyak M, Kaschak M. Experimental Emphysema: Its Production with Papain in Normal and Silicotic Rats. *Arch Environ Health*. 1965;(11):50-58.

56. Lucey EC, Keane J, Kuang P-P, Snider GL, Goldstein RH. Severity of Elastase-Induced Emphysema Is Decreased in Tumor Necrosis Factor-α and Interleukin-1β Receptor-Deficient Mice. *Lab Investig*. 2002;82(1):79-85. doi:10.1038/labinvest.3780397.

57. Limjunyawong N, Craig JM, Lagassé HAD, Scott AL, Mitzner W. Experimental progressive emphysema in BALB/cJ mice as a model for chronic alveolar destruction in humans. *Am J Physiol - Lung Cell Mol Physiol*. 2015;309(7):L662-L676. doi:10.1152/ajplung.00214.2015.

58. SCIREQ. flexiVent Techniques & Measurements. http://www.scireq.com/flexivent/techniques-and-measurements. Accessed January 3, 2016.

59. Hantos, Z; Daroczy, B; Suki, B; Daróczy, B; Suki, B; Nagy, S; Fredberg, JJ; Daroczy B. Input impedance and peripheral inhomogeneity of dog lungs. *J Appl Physiol*. 1992;72(1):168-178. http://jap.physiology.org/content/jap/72/1/168.full.pdf\nhttp://www.ncbi.nlm.nih.gov/pubmed/1537711.

60. Xu C, Hesselbacher S, Tsai C-L, et al. Autoreactive T Cells in Human Smokers is Predictive of Clinical Outcome. *Front Immunol*. 2012;3(August):267. doi:10.3389/fimmu.2012.00267.

61. D'hulst AI, Maes T, Bracke KR, et al. Cigarette smoke-induced pulmonary emphysema in scid-mice. Is the acquired immune system required? *Respir Res*. 2005;6:147. doi:10.1186/1465-9921-6-147.

62. Wickenden JA, Clarke MCH, Rossi AG, et al. Cigarette Smoke Prevents Apoptosis through Inhibition of Caspase Activation and Induces Necrosis. *Am J Respir Cell Mol Biol*. 2003;29(5):562-570. doi:10.1165/rcmb.2002-0235OC.

63. Churg A, Zay K, Shay S, et al. Acute cigarette smoke-induced connective tissue breakdown requires both neutrophils and macrophage metalloelastase in mice. *Am J Respir Cell Mol Biol*. 2002;27(3):368-374. doi:10.1165/rcmb.4791.

64. Bianchi ME. DAMPs, PAMPs and alarmins: all we need to know about danger. *J Leukoc Biol*. 2007;81(1):1-5. doi:10.1189/jlb.0306164.

65. Kaur M, Singh D. Neutrophil Chemotaxis Caused by Chronic Obstructive Pulmonary Disease Alveolar Macrophages: The Role of CXCL8 and the Receptors CXCR1/CXCR2. *J Pharmacol Exp Ther*. 2013;347(1):173-180. doi:10.1124/jpet.112.201855.

66. Mills PR, Davies RJ, Devalia JL. Airway epithelial cells, cytokines, and pollutants. *Am J Respir Crit Care Med*. 1999;160(5 Pt 2):S38-S43. doi:10.1164/ajrccm.160.supplement_1.11.

67. Gardi C, Stringa B, Martorana PA. Animal models for anti-emphysema drug discovery. *Expert Opin Drug Discov*. 2015;0441(January). doi:10.1517/17460441.2015.1016871.

68. Finlay GA, Odriscoll LR, Russell KJ, et al. Matrix metalloproteinase expression and production by alveolar macrophages in emphysema. *Am J Resp Crit Care Med*. 1997;156(1):240-247.

69. Elkington PTG, Friedland JS. Matrix metalloproteinases in destructive pulmonary pathology. *Thorax*. 2006;61(August 2008):259-266. doi:10.1136/thx.2005.051979.

70. Owen CA. Proteinases and oxidants as targets in the treatment of chronic obstructive pulmonary disease. *Proc Am Thorac Soc*. 2005;2(4):373-385; discussion 394-395. doi:10.1513/pats.200504-029SR.

71. Cornelius L a, Nehring LC, Harding E, et al. Matrix metalloproteinases generate angiostatin: effects on neovascularization. *J Immunol*. 1998;161(12):6845-6852. http://www.ncbi.nlm.nih.gov/pubmed/9862716.

72. Kukkonen MK, Tiili E, Vehmas T, Oksa P, Piirilä P, Hirvonen A. Association of genes of protease-antiprotease balance pathway to lung function and emphysema subtypes. *BMC Pulm Med*. 2013;13:36. doi:10.1186/1471-2466-13-36.

73. Russell RE, Culpitt S V, DeMatos C, et al. Release and activity of matrix metalloproteinase-9 and tissue inhibitor of metalloproteinase-1 by alveolar macrophages from patients with chronic obstructive pulmonary disease. *Am J Respir Cell Mol Biol*. 2002;26(13):602-609. doi:10.1165/ajrcmb.26.5.4685.

74. Vernooy JHJ, Lindeman JHN, Jacobs JA, Wouters EFM. Increased Activity of Matrix Metalloproteinase-8 and Matrix Metalloproteinase-9 in Induced Sputum From Patients With COPD * Increased Activity of Matrix Metalloproteinase-8 and Matrix Metalloproteinase-9 in Induced

Sputum From Patients With COPD *. 2004. doi:10.1378/chest.126.6.1802.

75. Yao H, Hwang J, Sundar IK, et al. SIRT1 redresses the imbalance of tissue inhibitor of matrix metalloproteinase-1 and matrix metalloproteinase-9 in the development of mouse emphysema and human COPD. *Am J Physiol Lung Cell Mol Physiol*. 2013;305(9):L615-L624. doi:10.1152/ajplung.00249.2012.

76. Mak JCW. Pathogenesis of COPD. Part II. Oxidative-antioxidative imbalance. *Int J Tuberc Lung Dis*. 2008;12(4):368-374.

77. Yao H, Arunachalam G, Hwang J, et al. Extracellular superoxide dismutase protects against pulmonary emphysema by attenuating oxidative fragmentation of ECM. *Proc Natl Acad Sci U S A*. 2010;107(35):15571-15576. doi:10.1073/pnas.1007625107.

78. Singh A, Rangasamy T, Thimmulappa RK, et al. Glutathione Peroxidase 2, the Major Cigarette Smoke–Inducible Isoform of GPX in Lungs, Is Regulated by Nrf2. *Am J Respir Cell Mol Biol*. 2006;35(6):639-650. doi:10.1165/rcmb.2005-0325OC.

79. Ware LB, Matthay MA. Keratinocyte and hepatocyte growth factors in the lung: roles in lung development, inflammation, and repair. *Am J Physiol - Lung Cell Mol Physiol*. 2002;282(5):L924-L940. http://ajplung.physiology.org/content/282/5/L924.abstract.

80. Ishizawa K, Kubo H, Yamada M, et al. Hepatocyte growth factor induces angiogenesis in injured lungs through mobilizing endothelial progenitor cells. *Biochem Biophys Res Commun*. 2004;324(1):276-280. doi:10.1016/j.bbrc.2004.09.049.

81. Noordhoek JA, Postma DS, Chong LL, et al. Different proliferative capacity of lung fibroblasts obtained from control subjects and patients with emphysema. *Exp Lung Res*. 2003;29. doi:10.1080/01902140303789.

82. Müller K-C, Welker L, Paasch K, et al. Lung fibroblasts from patients with emphysema show markers of senescence in vitro. *Respir Res*. 2006;7(1):1-10. doi:10.1186/1465-9921-7-32.

83. Holz O, Zühlke I, Jaksztat E, et al. Lung fibroblasts from patients with emphysema show a reduced proliferation rate in culture. *Eur Respir J*. 2004;24. doi:10.1183/09031936.04.00143703.

84. Nobukuni S, Watanabe K, Inoue J, Wen FQ, Tamaru N, Yoshida M. Cigarette smoke inhibits the growth of lung fibroblasts from patients with pulmonary emphysema. *Respirology*. 2002;7. doi:10.1046/j.1440-1843.2002.00400.x.

85. Plantier L, Marchand-adam S, Lese G, et al. Defect of hepatocyte growth factor production by fibroblasts in human pulmonary emphysema. 2005:641-647. doi:10.1152/ajplung.00249.2004.

86. Togo S, Holz O, Liu X, et al. Lung fibroblast repair functions in patients with chronic obstructive pulmonary disease are altered by multiple mechanisms. *Am J Respir Crit Care Med*. 2008;178(3):248-260. doi:10.1164/rccm.200706-929OC.

87. Peleman R a, Rytilä PH, Kips JC, Joos GF, Pauwels R a. The cellular composition of induced sputum in chronic obstructive pulmonary disease. *Eur Respir J*. 1999;13(4):839-843. http://www.ncbi.nlm.nih.gov/pubmed/10362050.

88. Keatings VM, Barnes PJ. Granulocyte activation markers in induced sputum: comparison between chronic obstructive pulmonary disease, asthma, and normal subjects. *Am J Respir Crit Care Med*. 1997;155(2):449-453. doi:10.1164/ajrccm.155.2.9032177.

89. Barnes P. Mediators of chronic obstructive pulmonary disease. *Pharmacol Rev*. 2004;56(4):515-548. doi:10.1124/pr.56.4.2.515.

90. Demirjian L, Abboud RT, Li H, Duronio V. Acute effect of cigarette smoke on TNF-alpha release by macrophages mediated through the erk1/2 pathway. *Biochim Biophys Acta*. 2006;1762(6):592-597. doi:10.1016/j.bbadis.2006.04.004.

91. Yang S, Chida AS, Bauter MR, et al. Cigarette smoke induces proinflammatory cytokine release by activation of NF-κB and posttranslational modifications of histone deacetylase in macrophages. *Am J Physiol - Lung Cell Mol Physiol*. 2006;291(1):L46-L57. doi:10.1152/ajplung.00241.2005.

92. Murray PJ, Wynn TA. Protective and pathogenic functions of macrophage subsets. *Nat Rev Immunol*. 2011;11(11):723-737. doi:10.1038/nri3073.

93. Ramachandran P, Iredale JP, Fallowfield JA. Resolution of Liver Fibrosis: Basic Mechanisms and Clinical Relevance. *Semin Liver Dis*. 2015;35(02):119-131. doi:10.1055/s-0035-1550057.

94. Lesnik P, Haskell C a, Charo IF. Decreased atherosclerosis in CX 3 CR1 –/– mice reveals a role for fractalkine in atherogenesis. 2003;111(3):333-340. doi:10.1172/JCI200315555.Introduction.

95. Tsujioka H, Imanishi T, Ikejima H, et al. Impact of Heterogeneity of Human Peripheral Blood Monocyte Subsets on Myocardial Salvage in Patients With Primary Acute Myocardial Infarction. *J Am Coll Cardiol*. 2009;54(2):130-138. doi:10.1016/j.jacc.2009.04.021.

96. Misharin A V., Cuda CM, Saber R, et al. Nonclassical Ly6C- monocytes drive the development of inflammatory arthritis in mice. *Cell Rep*. 2014;9(2):591-604. doi:10.1016/j.celrep.2014.09.032.

97. Pappas K, Papaioannou AI, Kostikas K, Tzanakis N. The role of macrophages in obstructive airways disease: Chronic obstructive pulmonary disease and asthma. *Cytokine*. 2013;64(3):613-625. doi:10.1016/j.cyto.2013.09.010.

98. Boorsma CE, Draijer C, Melgert BN. Macrophage heterogeneity in respiratory diseases. *Mediators Inflamm*. 2013;2013. doi:10.1155/2013/769214.

99. Liew F. Cigarette smoke resets the alarmin IL-33 in COPD. *Immunity*. 2015;42(3):401-403. doi:10.1016/j.immuni.2015.02.014.

100. Martin NT, Martin MU. Interleukin 33 is a guardian of barriers and a local alarmin. *Nat Immunol*. 2016;17(2):122-131. doi:10.1038/ni.3370.

101. Rooijen N Van, Hendrikx E. Liposomes for Specific Depletion of Macrophages from Organs and Tissues. In: Vol 605. ; 2010:189-203. doi:10.1007/978-1-60327-360-2.

102. Limjunyawong N, Fallica J, Ramakrishnan A, et al. Phenotyping mouse pulmonary function in vivo

with the lung diffusing capacity. *J Vis Exp*. 2015;95:e52216. doi:10.3791/52216.

103. Ewart S, Levitt R, Mitzner W. Respiratory system mechanics in mice measured by end-inflation occlusion. *J Appl Physiol*. 1995;79(2):560-566.

104. Limjunyawong N, Fallica J, Horton M, Mitzner W. Measurement of the pressure-volume curve in mouse lungs. *J Vis Exp*. 2015;95:e52376. doi:10.3791/52376.

105. Bucher K, Schmitt F, Autenrieth SE, et al. Fluorescent Ly6G antibodies determine macrophage phagocytosis of neutrophils and alter the retrieval of neutrophils in mice. *J Leukoc Biol*. 2015;98(3):365-372. doi:10.1189/jlb.1AB1014-488RR.

106. Beamer CA, Holian A. Antigen-presenting cell population dynamics during murine silicosis. *Am J Respir Cell Mol Biol*. 2007;37(6):729-738. doi:10.1165/rcmb.2007-0099OC.

107. Thepen BT, Rooijen NVAN, Kraal G. ALVEOLAR MACROPHAGE ELIMINATION IN VIVO IS ASSOCIATED WITH AN INCREASE IN PULMONARY IMMUNE RESPONSE IN MICE Exposure to a wide variety of antigens in ambient air takes place almost continu- ously via the lung . As the main part ofthese antigens are trivia. 1989;170(August).

108. Johansson A, Lundborg M, Skold CM, et al. Functional, Morphological, and Phenotypical Differences Between Rat Alveolar and Interstitial Macrophages. *Am J Respir Cell Mol Biol*. 1997;16(5):582-588. doi:10.1006/exmp.2000.2344.

109. Barjaktarevic I, Springmeyer S, Gonzalez X, Sirokman W, Coxson HO, Cooper CB. Diffusing Capacity for Carbon Monoxide Correlates Best With Tissue Volume From Quantitative CT Scanning Analysis. *CHEST J*. 2015;147(6):1485. doi:10.1378/chest.14-1693.

110. Ferguson GT. Why does the lung hyperinflate? *Proc Am Thorac Soc*. 2006;3(2):176-179. doi:10.1513/pats.200508-094DO.

111. Misharin A V., Morales-Nebreda L, Mutlu GM, Budinger GRS, Perlman H. Flow cytometric analysis of

macrophages and dendritic cell subsets in the mouse lung. *Am J Respir Cell Mol Biol*. 2013;49(4):503-510. doi:10.1165/rcmb.2013-0086MA.

112. Zaynagetdinov R, Sherrill TP, Kendall PL, et al. Identification of myeloid cell subsets in murine lungs using flow cytometry. *Am J Respir Cell Mol Biol*. 2013;49(2):180-189. doi:10.1165/rcmb.2012-0366MA.

113. Mancardi DA, Albanesi M, Jönsson F, et al. The high-affinity human IgG receptor FcγRI (CD64) promotes IgG-mediated inflammation, anaphylaxis, and antitumor immunotherapy. *Blood*. 2013;121(9):1563-1573. doi:10.1182/blood-2012-07-442541.

114. Ziegler-Heitbrock L. Blood monocytes and their subsets: Established features and open questions. *Front Immunol*. 2015;6(AUG):1-5. doi:10.3389/fimmu.2015.00423.

115. Ginhoux F, Jung S. Monocytes and macrophages: developmental pathways and tissue homeostasis. *Nat Rev Immunol*. 2014;14(6):392-404. doi:10.1038/nri3671.

116. Ramachandran P, Pellicoro A, Vernon M a, et al. Differential Ly-6C expression identifies the recruited macrophage phenotype, which orchestrates the regression of murine liver fibrosis. *Proc Natl Acad Sci U S A*. 2012;109(46):E3186-E3195. doi:10.1073/pnas.1119964109.

117. Nahrendorf M, Swirski FK, Aikawa E, et al. The healing myocardium sequentially mobilizes two monocyte subsets with divergent and complementary functions. *J Exp Med*. 2007;204(12):3037-3047. doi:10.1084/jem.20070885.

118. Wang J, Huang WL, Wang C, Liu RY. Dynamic process of phagocytosis and forms of macrophage cell death induced by ingestion of apoptotic neutrophils. *Sci China Life Sci*. 2014;57(10):1018-1023. doi:10.1007/s11427-014-4726-y.

119. Lee HN, Surh YJ. Resolvin D1-mediated NOX2 inactivation rescues macrophages undertaking efferocytosis from oxidative stress-induced apoptosis. *Biochem Pharmacol*. 2013;86(6):759-769. doi:10.1016/j.bcp.2013.07.002.

120. Morimoto K, Amano H, Sonoda F, et al. Alveolar macrophages that phagocytose apoptotic neutrophils produce hepatocyte growth factor during bacterial pneumonia in mice. *Am J Respir Cell Mol Biol*. 2001;24(5):608-615. doi:10.1165/ajrcmb.24.5.4292.

121. Moransard M, Sawitzky M, Fontana A, Suter T. Expression of the HGF receptor c-met by macrophages in experimental autoimmune encephalomyelitis. *Glia*. 2010;58(5):559-571. doi:10.1002/glia.20945.

122. Karo-Atar D, Moshkovits I, Eickelberg O, K??nigshoff M, Munitz A. Paired immunoglobulin-like receptor-B inhibits pulmonary fibrosis by suppressing profibrogenic properties of alveolar macrophages. *Am J Respir Cell Mol Biol*. 2013;48(4):456-464. doi:10.1165/rcmb.2012-0329OC.

123. Schultze JL. Reprogramming of macrophages—new opportunities for therapeutic targeting. *Curr Opin Pharmacol*. 2016;26:10-15. doi:10.1016/j.coph.2015.09.007.

124. Sica A, Mantovani A. Macrophage plasticity and polarization: In vivo veritas. *J Clin Invest*. 2012;122(3):787-795. doi:10.1172/JCI59643.

125. Ma SF, Chen YJ, Zhang JX, et al. Adoptive transfer of M2 macrophages promotes locomotor recovery in adult rats after spinal cord injury. *Brain Behav Immun*. 2015;45:157-170. doi:10.1016/j.bbi.2014.11.007.

126. Fleming BD, Chandrasekaran P, Dillon LAL, et al. The generation of macrophages with anti-inflammatory activity in the absence of STAT6 signaling. *J Leukoc Biol*. 2015;98(3):395-407. doi:10.1189/jlb.2A1114-560R.

127. Suzuki T, Arumugam P, Sakagami T, et al. Pulmonary macrophage transplantation therapy. *Nature*. 2014;514(7523):450-454. doi:10.1038/nature13807.

128. Happle C, Lachmann N, Skuljec J, et al. Pulmonary transplantation of macrophage progenitors as effective and long-lasting therapy for hereditary pulmonary alveolar proteinosis. *Sci Transl Med*. 2014;6(250):250ra113. doi:10.1126/scitranslmed.3009750.

129. Johnson CP, Edmiston Jr. CE, Zhu YR, Adams MB, Roza AM, Kurup V. A murine model of invasive aspergillosis: variable benefit of interferon-gamma administration under in vitro and in vivo conditions. *Surg Infect*. 2005;6(4):397-407. doi:10.1089/sur.2005.6.397.

130. D'Alessio FR, Craig JM, Singer BD, et al. Enhanced Resolution of Experimental ARDS through IL-4-Mediated Lung Macrophage Reprogramming. *Am J Physiol - Lung Cell Mol Physiol*. 2016;1(20):ajplung.00419.2015. doi:10.1152/ajplung.00419.2015.

131. Agrawal A, Manchester M. Differential uptake of chemically modified cowpea mosaic virus nanoparticles in macrophage subpopulations present in inflammatory and tumor microenvironments. *Biomacromolecules*. 2012;13(10):3320-3326. doi:10.1021/bm3010885.

**Amy K Poupore**
15 N Belnord Avenue • Baltimore, Maryland 21224
apoupor1@jhu.edu • 410.207.8962

**Education**

Master of Science – Molecular Microbiology and Immunology
Johns Hopkins Bloomberg School of Public Health – Baltimore, Maryland, May 2016

Bachelor of Science – Bioinformatics, concentration in genomics
Minor in chemistry
*Magna cum laude*
Virginia Commonwealth University - Richmond, Virginia, May 2012

**Laboratory Skills**

Rodent handling
Multicolor flow cytometry
Basic parasitology
Protein and nucleic acid isolation
Western blotting
Standard and RT PCR
DNA cloning with plasmid vector
Bone marrow isolation

**Computer Skills**

Proficiency: FlowJo, FACSDiva, CellQuest Pro, STATA, Microsoft Office, EpicCare EMR
Educational experience: R, PERL, Java, SQL, Unix

**Research Experience**

*Master's thesis, Department of Molecular Microbiology and Immunology, Johns Hopkins Bloomberg School of Public Health*

Research advisor: Alan Scott, PhD; 2014-present

- Designed and optimized a 10-color flow cytometry panel to discriminate between myeloid cell subsets in the elastase-induced murine model of progressive emphysema
- Evaluated the role of macrophages in the progression of emphysema

*Research assistant, Department of Surgery, Johns Hopkins University School of Medicine*

Research advisor: Anne Lidor, MD, MPH; 2014-present

- Outcomes-based research on patients undergoing upper gastrointestinal surgery
- Recent projects include: readmission following benign distal esophageal disease surgery, adherence to National Comprehensive Cancer Network guidelines and esophagectomy outcomes, and quality of life following paraesophageal hernia repair.

*Molecular genetics laboratory (course), Center for the Study of Biological Complexity, Virginia Commonwealth University*

Professor: Luis Ozaki, PhD; 2012

- Led team in applying molecular genetics techniques and genomic analysis software in the species identification and midgut microflora analysis of wild-caught mosquitoes

*Applications in bioinformatics (course), Center for the Study of Biological Complexity, Virginia Commonwealth University*

Professor: Luis Ozaki, PhD; 2012

- Led a team of three in the design and implementation of an experiment to evaluate host range and degree of synonymous codon usage bias in influenza

- Met analytical objectives by developing programs in PERL and R and sought out, learned, and applied bioinformatics tools to analyze over 33,000 DNA sequences

*Introduction to bioinformatics (course), Center for the Study of Biological Complexity, Virginia Commonwealth University*

Professor: Jeffrey Elhai, PhD; 2011

- Wrote programs in BioBike and applied BLAST to identify sequences of novel candidate transposable elements in the genome of mycobacteriophage Wally

*Howard Hughes Medical Institute Summer Scholars, Mechanical Engineering Department, Virginia Commonwealth University*

Research advisor: Amy Throckmorton, PhD; 2009

- With minimal instruction, learned and applied the design software SolidWorks to create prospective blood pumps
- Collaborated with lab members to evaluate the hydraulic performance and hemolysis of each prospective pump

## Publications

**Poupore AK**, Stem M, Molena D, Lidor AO. Incidence, Reasons, and Risk Factors for Readmission Following Surgery for Benign Distal Esophageal Disease. *SURGERY*. Under review.

Lagassé HAD, Anidi IU, Craig JM, Limjunyawong N, **Poupore AK**, Mitzner W, Scott AL. Recruited Monocytes Modulate Malaria-Induced Lung Injury Through CD36-Mediated Clearance of Sequestered Infected Erythrocytes. *Journal of Leukocyte Biology*. 2015, ePub ahead of print. doi: 10.1189/jlb.4HI0315-130RRR.

Molena D, Mungo B, Stem M, **Poupore AK**, Chen SY, Lidor AO. Does Quality of Care Matter? A Study of Adherence to National Comprehensive Cancer Network Guidelines for Patients with Locally Advanced Esophageal Cancer. *Journal of Gastrointestinal Surgery*. 2015; ePub ahead of print. doi: 10.1007/s11605-015-2899-8

Kapadia JY, Pierce KC, **Poupore AK**, Throckmorton AL. Hydraulic Testing of Intravascular Axial Flow Blood Pump Designs with a Protective Cage of Filaments for Mechanical Cavopulmonary Assist. *ASAIO J*. 2010; 56: 17-23. doi: 10.1097/MAT.0b013e3181c5b046

## Presentations

**Poupore AK**, Stem M, Molena D, Lidor AO. Incidence, Reasons, and Risk Factors for Readmission Following Surgery for Benign Distal Esophageal Disease. Oral presentation at the 11th Annual Academic Surgical Congress. 2016 Feb 2-4, Jacksonville, FL.

**Poupore AK,** Nguyen T, Stevenson D. Identification of Novel Candidate Transposable Elements in Mycobacteriophage Wally. Oral presentation at the 2nd Annual VCU Symposium on Mycobacteriophage Genomes. 2011 May 2, Richmond, VA.